



## **Non-Gaussian, non-ergodic, and non-Fickian diffusion of tracers in mucin hydrogels**

Journal:	<i>Soft Matter</i>
Manuscript ID	SM-ART-10-2018-002096.R1
Article Type:	Paper
Date Submitted by the Author:	20-Dec-2018
Complete List of Authors:	Cherstvy, Andrey; Institut für Festkörperforschung, biological soft matter physics Thapa, Samudrajit; University of Potsdam, Inst for Physics & Astronomy Wagner, Caroline; Princeton University Department of Molecular Biology Metzler, Ralf; University of Potsdam, Inst for Physics & Astronomy

# Non-Gaussian, non-ergodic, and non-Fickian diffusion of tracers in mucin hydrogels

Andrey G. Cherstvy<sup>\*,1,\*</sup> Samudrajit Thapa,<sup>1,†</sup> Caroline E. Wagner,<sup>2,3,‡</sup> and Ralf Metzler<sup>\*,1,§</sup>

<sup>1</sup>*Institute for Physics & Astronomy, University of Potsdam, 14476 Potsdam-Golm, Germany*

<sup>2</sup>*Dept of Mechanical Engineering, Massachusetts Institute of Technology, Cambridge, Massachusetts 02139, United States*

<sup>3</sup>*Dept of Ecology and Evolutionary Biology, Princeton University, Princeton, New Jersey 08544, United States*

(Dated: January 28, 2019)

Native mucus is polymer-based soft-matter material of paramount biological importance. How non-Gaussian and non-ergodic is the diffusive spreading of pathogens in mucus? We study the passive, thermally driven motion of micron-sized tracers in hydrogels of mucins, the main polymeric component of mucus. We report the results of the Bayesian analysis for ranking several diffusion models for a set of tracer trajectories [C. E. Wagner et al., *Biomacromol.* **18**, 3654 (2017)]. The models with "diffusing diffusivity", fractional and standard Brownian motion are used. The likelihood functions and evidences of each model are computed, ranking the significance of each model for individual traces. We find that viscoelastic anomalous diffusion is often most probable, followed by Brownian motion, while the model with a diffusing diffusion coefficient is only realised rarely. Our analysis also clarifies the distribution of time-averaged displacements, correlations of scaling exponents and diffusion coefficients, and the degree of non-Gaussianity of displacements at varying pH levels. Weak ergodicity breaking is also quantified. We conclude that—consistent with the original study—diffusion of tracers in the mucin gels is most non-Gaussian and non-ergodic at low pH that corresponds to the most heterogeneous networks. Using the Bayesian approach with the nested-sampling algorithm, together with the quantitative analysis of multiple statistical measures, we report new insights into possible physical mechanisms of diffusion in mucin gels.

## I. INTRODUCTION

### A. Biological significance of native-mucus films

Mucus hydrogels are ubiquitous in animal biology, being quintessential for the survival of animals of multiple classes (tetrapoda (mammals, amphibians, reptiles, birds), marine invertebrates, etc.). Sticky polymer-based mucus films are robust and selectively-permeable filters that maintain tissue-protective barriers<sup>1–21</sup> with intricate physico-chemical properties, performance-optimisation strategies, and functioning mechanisms. Native mucus forms renewable layers on many surfaces in the human body not protected by "dry" epithelium<sup>22</sup>. These water-based (92-98% of water content) polymeric hydrogels with  $\sim 1 \dots 5$  wt % of mucin-glycoprotein<sup>13</sup> coat "moist"-epithelial surfaces. Additional mucus constituents are ions, lipids, proteins, and DNA<sup>8,18,23</sup>. Mucus is present in the eye (vitreous humour<sup>17</sup>) and oral (saliva<sup>10,24–26</sup>) cavities, in the respiratory tract (lungs<sup>2,10,23</sup>, sputum in bronchi, nasal airways<sup>3,6,12,27</sup>), gastrointestinal (stomach and intestine<sup>1,4,7,28–31</sup>) and female genital tract (cervico-vaginal mucus<sup>9,11,15,17,32</sup>), see Fig. 1a and Refs.<sup>13,20</sup>.

In the stomach and lungs, the mucosal surface ensures protection from harmful molecules and pathogens. In the lungs, via the cilia-beating mechanism<sup>2</sup>, the mucus film establishes an active "transportation" of inhaled particles—pollutants, allergens, toxic agents, dust, pathogens<sup>8</sup>, viruses<sup>9,18,22,26</sup>, bacteria<sup>22</sup>, etc.—out of the body<sup>2</sup>. Hypersecretion and/or dehydration of mucus gels contribute crucially to chronic airways diseases, such as asthma, bronchitis, cystic fibrosis<sup>5,8,16,27,33</sup>, and chronic obstructive pulmonary disease<sup>2,12</sup>. Enteric infections of the intestine present major health problems, in the

industrialised and developing world<sup>1,31</sup>. The bacterial pathogen *Helicobacter pylori* colonises a sizeable part of the human population (stomach), causing inflammation and gastrointestinal disease<sup>4,10</sup>, and, possibly, also triggering gastric cancer<sup>31,169</sup>. Mucus films on the surfaces of internal organs serve as effective lubricants<sup>8,25</sup>. These examples underline the paramount importance of mucus, Fig. 1a, making it a popular subject of biological, biophysical, and statistical physics research. This research has accelerated in recent years due to the experimental exploration of various aspects of the functioning of native mucus and of hydrogels of purified mucins, and the quantification of these results by statistical measures and theoretical models.

Due to "mucoadhesion"<sup>6,10,18</sup>, mucus layers can trap and neutralise virus-like particles smaller than the meshwork size (down to  $\sim 50$  nm<sup>9</sup>). Conversely, considerably bigger but non-sticky particles can still diffuse through the mucus layer<sup>1</sup>. The addition of salt strengthens the protective properties of mucus against the penetration of viruses<sup>9</sup>. The permeability of mucus depends on a typical mesh-size of the mucin network, the types of physical tracer-gel interactions involved, on external conditions, and, clearly, on tracer size, see Sec. V C. Moreover, the thickness of mucus varies between tissues and organs<sup>1,10,14,17,31</sup>, as does the wt % of mucins.

Pathogens, in turn, invent different strategies to reduce their binding to mucin chains—for instance, by degrading/disrupting mucus films<sup>18</sup> or changing the viscoelastic properties of mucus<sup>31</sup>—to ease penetration through the protective layer<sup>1,17,28</sup>. The diffusion of pathogens and other molecules of varying chemical structure and surface composition<sup>18</sup> in mucin gels<sup>10</sup> provides experimental evidences required, e.g., to optimise strategies of drug/gene

delivery through mucus layers<sup>8,15,17,18,34,35</sup> (see Ref.<sup>36</sup> for the perspective on injectable biodegradable hydrogels for drug delivery). For instance, a number of macro- and micro-rheological<sup>37,38</sup> measurements on mucus (in bulk and on thin films) have been performed over the last few decades<sup>8</sup> to unravel its mechanical and viscoelastic properties as well as the response characteristics.<sup>170</sup>

## B. Mucins and structural analysis of their networks

Mucin is the major constituent of mucus with a high molecular weight<sup>18,20,25</sup>. At neutral conditions (pH=7) mucin chains are negatively charged glycoproteins which interact via hydrophobic and electrostatic<sup>39,40</sup> forces as well as via the formation of disulfide bonds<sup>20,30</sup>. There-

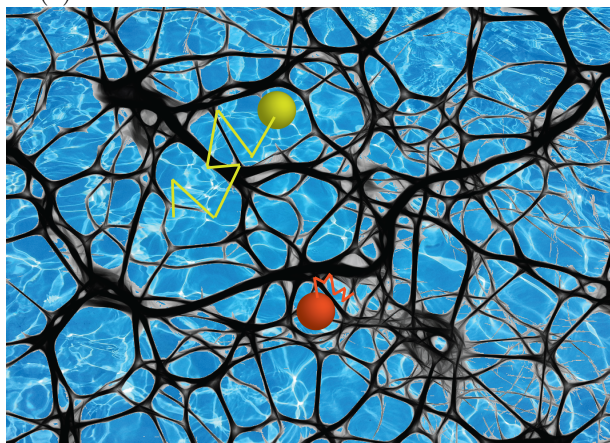
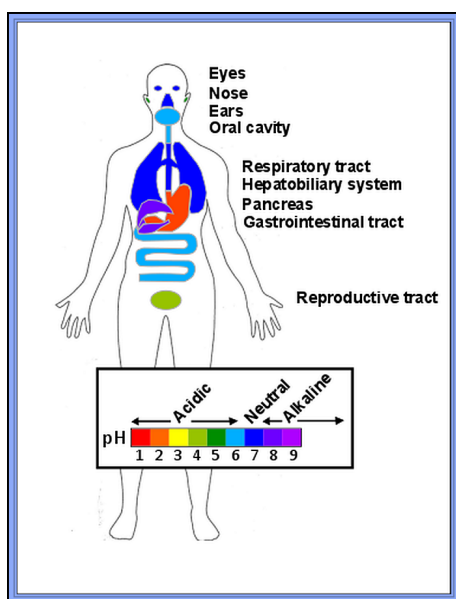


FIG. 1: (a) Mucus films in the human body, with their respective pH conditions. The image is reproduced from Ref.<sup>26</sup> (Open-Access domain). (b) Artistic view of polymer-confined and diffusing tracers in strongly heterogeneous mucin hydrogels (background images: source files courtesy pixabay.com).

fore, it is not surprising that many positively charged (sub)micron-sized particles get trapped in mucus gels<sup>18</sup>. Particle–gel binding is one physical mechanism of hindrance of pathogen propagation in polymer films<sup>14,22,41</sup>, see also Refs.<sup>42,43</sup>. At pH=2, the mucins are close to neutrally charged and extended (as compared to a coil-like<sup>20</sup> shape at pH=7). Mucin chains can chemically crosslink; their oligomers<sup>25</sup> polymerise up to giant molecular weights,  $MW \sim 50 \dots 100 \text{ MDa}$ <sup>19</sup>, via end-to-end disulfide bonds. This results in complex polymer networks<sup>8,10,12,20</sup> with rich internal dynamics over several timescales, see, e.g., Fig. 4 in Ref.<sup>10</sup>. The permeability of such a network to thermally-agitated and actively driven tracers is controlled by size- and interaction-dependent mechanisms, see Refs.<sup>2,6,7,10,12,17,18,20,26</sup> for a discussion. Additionally, mucosal surfaces can host a number of bacteriophages which—via performing *subdiffusive* motion—optimise their search strategies for external bacteria in the limit of *rare* phage–host encounters<sup>16</sup>.

The family of secreted mucins contains oligomeric gel-forming (MUC2, MUC5AC, MUC5B, MUC6, and MUC19) and nonpolymeric (MUC7 and MUC8) glycoproteins<sup>1,2,12,26</sup>. Each of them has specific physicochemical and material characteristics, affecting tracer diffusion in respective gels<sup>10,12,17,20,25</sup>. In recent years, the properties of translocation of tracers and virus-like particles in mucin gels<sup>17</sup> were explored in a number of experiments<sup>5–7,10,13–17,19,20,25,27,34</sup>, e.g., via single-particle tracking (SPT)<sup>47,48</sup> and subsequent single-trajectory data analysis.<sup>171</sup> Tracer diffusion in gels of MUC5AC<sup>9</sup> was studied in detail recently<sup>19,20</sup> (see Sec. III below and Fig. 2). The data of Refs.<sup>19,20</sup> provide the experimental basis for the statistical and Bayesian analysis below, the main focus of the current study.

## C. Structure of the paper

The paper is organised as follows. In Sec. II A we introduce the theoretical quantifiers for the data analysis. In Sec. II B we shortly overview the concepts of stochastic diffusivity, superstatistical viewpoint, and the Bayesian model-ranking approach. In Sec. III we overview the features of diffusion of tracers of different sizes, under varying conditions, and subject to different measurement protocols in mucin gels, as examined in Refs.<sup>19,20</sup>. In Sec. IV the main findings of the model-ranking and statistical data-analysis results are presented. They include the results of the Bayesian approach (Sec. IV A), the evaluation of time-averaged displacements,  $\overline{\delta_i^2}$  (Sec. IV B), the distribution of scaling exponents  $\beta_i$  and diffusion coefficients  $(K_\beta)_i$  of time-averaged displacements, the extent of  $K_\beta$ – $\beta$  correlations (Sec. IV C), the ergodicity breaking parameter (Sec. IV D), the non-Gaussian PDFs of displacements (Sec. IV E), and, finally, displacement auto-correlations (Sec. IV F). These quantifiers can be used, e.g., to characterise medium heterogeneities and determine the most relevant model of diffusion. In Sec. V the

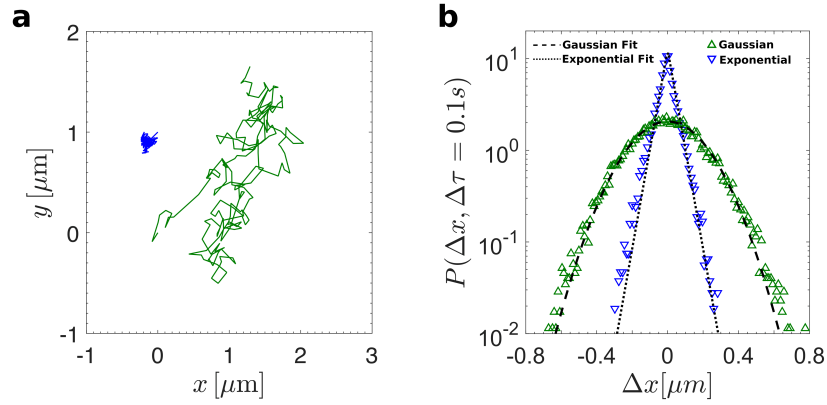


FIG. 2: (a) Two trajectories of micron-sized tracers diffusing in mucin gels, as recorded in the experiment #2 of Ref. <sup>19</sup> at pH=2. The timescale in experiments is 0.1 sec. Panel (b) illustrates the respective distributions of displacements for fast (Gaussian, green colour in both panels) and slow (exponential, blue colour) tracers. Separation of particles into two subpopulations and fitting procedure are described in Sec. III and Eq. (10). Video files of real-time tracking are provided in the Supplementary Material (camera framerate is  $\approx 30$  fps). Some particles (the green one in the video) diffuse more readily than others (the red and white tracers). The scale bar in the video is  $50 \mu\text{m}$ . The graph is adapted from Ref. <sup>19</sup> with permission (Copyright 2017, American Chemical Society).

results are discussed in the context of diffusion models consistent with the data<sup>19,20</sup>. In Sec. V C, we list certain aspects of this system that still remain to be understood. The details of the Bayesian model-ranking approach and the diffusion models employed are provided in Apps. A and B, respectively, whereas the supplementary figures are collected in App. C.

## II. PHYSICAL OBSERVABLES

### A. Anomalous diffusion, non-Gaussianity, and non-ergodicity

The hallmarks of normal diffusion are the linear growth of the mean-squared displacement (MSD) and the Gaussian distribution of particles' increments. Stochastic processes producing anomalous diffusion feature a nonlinear MSD scaling<sup>66,70–80</sup>, namely (in one dimension)

$$\langle [x(t) - x(0)]^2 \rangle = \int x^2 P(x, t) dx = 2K_\alpha t^\alpha \simeq t^\alpha. \quad (1)$$

Here  $\alpha$  is the anomalous scaling exponent,  $K_\alpha$  is the generalised diffusion coefficient, and  $P(x, t)$  is the probability density function (PDF) of particle displacements. The situation  $0 < \alpha < 1$  corresponds to subdiffusion, Brownian motion (BM) features  $\alpha = 1$ , while for  $1 < \alpha < 2$  superdiffusive spreading dynamics is realised (actively driven systems). Ballistic motion features  $\alpha = 2$ , whereas for hyperdiffusion we have  $\alpha > 2$ <sup>66,74,76,77</sup>. The latter may arise in non-stationary situations, for instance, for diffusion in heterogeneous systems<sup>81</sup>, under increasing temperature<sup>82</sup>, or in expanding media<sup>83</sup>. In what follows, the scaling exponent of the ensemble-averaged and

time-averaged displacements are denoted as  $\alpha$  and  $\beta_i$ , respectively, see Eqs. (1) and (11). In general, these two exponents are not identical for a potentially non-ergodic anomalous diffusion process<sup>66,74</sup>.

In addition to the MSD (1), the measure of spreading often used in SPT experiments is the time-averaged MSD (TAMSD), defined for a time series  $x_i(t)$  as<sup>66,73,74,77,79</sup>

$$\overline{\delta_i^2(\Delta)} = \frac{1}{T - \Delta} \int_0^{T - \Delta} [x_i(t + \Delta) - x_i(t)]^2 dt.$$

For an ensemble of  $N$  trajectories the mean TAMSD is

$$\langle \overline{\delta^2(\Delta)} \rangle = N^{-1} \sum_{i=1}^N \overline{\delta_i^2(\Delta)}. \quad (2)$$

Here,  $T$  is the total length of the trajectory and  $\Delta$  is the lag time (a sliding window for averaging along the trajectory). For SPT time series of the  $i$ th tracer, which is  $x_i(k \cdot dt)$  at time instance  $1 \leq k \leq N = T/dt$ , the TAMSD is the discrete analog of (2), namely

$$\overline{\delta_i^2(\tau)} = \frac{1}{N - \frac{\tau}{dt}} \sum_{k=1}^{N - \frac{\tau}{dt}} [x_i(k \cdot dt + \tau) - x_i(k \cdot dt)]^2. \quad (3)$$

The non-equivalence of the MSD and TAMSD gives rise to the phenomenon of weak ergodicity breaking<sup>66,73,74</sup>, see also Refs. <sup>84,85</sup>. Its measure—the ergodicity breaking parameter (EB)—quantifies the degree of irreproducibility or the dispersion (amplitude scatter) of individual TAMSD realisations. It is defined via the fourth moment

of displacements as<sup>66,73–75,86</sup>

$$\text{EB}(\Delta) = \left\langle \left( \overline{\delta^2(\Delta)} \right)^2 \right\rangle / \left\langle \overline{\delta^2(\Delta)} \right\rangle^2 - 1. \quad (4)$$

In addition to the non-ergodic behaviour of individual TAMSDs, for some stochastic processes the PDF can be substantially non-Gaussian<sup>66,67,87–89</sup>. We remind here that Gaussianity is expected for BM, with the PDF for a given  $D$  value after time  $t$  being

$$P(x, t; D) = \exp\left(-\frac{x^2}{4Dt}\right) / \sqrt{4\pi Dt}. \quad (5)$$

Fractional Brownian motion (FBM) with a fixed noise strength is also a Gaussian process<sup>66,74</sup>, while stochastic processes with scale-free waiting-time distributions are inherently non-Gaussian. The non-Gaussianity parameter<sup>66,77,90</sup> quantifies the degree of non-Gaussianity,

$$\kappa(t) = \langle x(t)^4 \rangle / 3 \langle x^2(t) \rangle^2 - 1. \quad (6)$$

Here, instead of the ensemble-averaged moments, the time-averaged moments can also be used<sup>42,91</sup>.

In recent years, the subject of tracer diffusion in entangled polymeric networks and in polymer nanocomposites attracted considerable attention from both theoretical and computer-simulation communities<sup>39,40,44,92–97</sup>, including some “gel on a brush” models<sup>2</sup>. Collapsing hydrogels<sup>99</sup> and the response of hydrogels to external stimuli<sup>43</sup> were explored. Notably, ageing *effects* of mucus viscoelasticity can be pronounced in certain systems<sup>20,30</sup> (see Secs. IV A and V C below; see also Ref.<sup>98</sup>).<sup>172</sup>

## B. Stochastic diffusivity and Bayesian analysis

Recently, the subject of trajectory-specific and stepnumber-dependent diffusivities gained a lot of attention from experimental, theoretical, and computational communities<sup>49,67,82,87–89,100–109,113</sup>. Mathematical models with linear MSD growth based on the “diffusing diffusivity” (DD) concept are possible candidates to rationalise non-Gaussian (often exponential) tails in displacement-distributions<sup>67</sup>. The latter were indeed detected in a number of SPT experiments, see, e.g., Refs.<sup>19,46,87–89,95,105–107,110–113</sup>. The model of BM with DD is, for instance, based on the Ornstein-Uhlenbeck (OU) process<sup>68,69</sup> that describes diffusion in a parabolic potential (see Ref.<sup>114</sup> for its ergodic properties). The current DD model was developed in a recent theoretical study<sup>67</sup> and included in the Bayesian model-ranking analysis using nested sampling in Ref.<sup>49</sup>.<sup>173</sup>

For instance, for the *stationary* exponential distribution of diffusion coefficients,  $\pi(D) = e^{-D/\langle D \rangle} / \langle D \rangle$ , as

proposed in Refs.<sup>89,100</sup>, the convolution of the form

$$P(x, t) = \int_0^\infty \pi(D) P(x, t; D) dD \quad (7)$$

with the Gaussian propagator for a given diffusivity, see Eq. (5), results in the exponential PDF of displacements,

$$P(x, t) = \int_0^\infty \pi(D) P(x, t; D) dD = e^{-\frac{|x|}{\sqrt{\langle D \rangle t}}} / \sqrt{4 \langle D \rangle t}. \quad (8)$$

The resulting MSD obeys Fick’s law of diffusion,

$$\langle x^2(t) \rangle = \int_{-\infty}^\infty x^2 P(x, t) dx = 2 \langle D \rangle t. \quad (9)$$

We refer to the recent study<sup>49</sup> where the superstatistical approach<sup>117,118</sup> for the DD model<sup>67</sup> and the Bayesian nested-sampling algorithm were described in detail and thoroughly tested for consistency, performance, model-significance predictions, and error bars. The general concepts of Bayesian statistics and nested sampling are detailed in Apps. A and B.

The mathematical model of BM—modified by the DD concept due to a variation of diffusion coefficients between the trajectories and also along each trajectory—reveals an increased spread of individual TAMSDs (2) as compared to BM, even for short lag times. This, in turn, is reflected in the EB parameter, see the inset of Fig. A1 and Fig. A2. We find that the EB parameter for the DD model—normalised to the respective EB value for BM—stays roughly constant. Thus, in the limit  $\Delta/T \ll 1$  it scales as  $\text{EB}_{\text{DD}}(T) \sim 1/T$  with the trace length, similar to BM and some anomalous diffusion processes<sup>66</sup>. Also, plotting the EB results from computer simulations for different lag times<sup>49</sup>, we find that  $\text{EB}_{\text{DD}}(\Delta)$  is considerably larger than  $\text{EB}_{\text{BM}}(\Delta)$  at short lag times  $\Delta$ , a feature of a less ergodic system, Fig. A2.

The Bayesian maximum-likelihood analysis<sup>50,62,119–122</sup> with the nested-sampling approach<sup>51–55,63</sup> is a well established technique to rank theoretical models for a given set of data based on their *relative* probabilities<sup>49,123</sup>. In particular, for SPT data the Bayesian approach combined with the nested-sampling algorithm was developed for FBM<sup>64,124</sup> and the DD model<sup>49,63</sup> (the computer codes are available<sup>125</sup>). We also accounted for some *measurement noise* potentially present for BM and FBM, in terms of errors in the particle-localisation procedure or due to external inaccuracy sources, see Ref.<sup>49</sup> for the algorithm. Our set of possible diffusion models for each SPT trajectory consists of BM, noisy BM, FBM, noisy FBM, and DD. For each trajectory, only models from this list can be chosen.

Our physical intuition, e.g., proposes that this system features certain viscoelastic properties and thus FBM can be a viable model. We also mention the Bayesian study<sup>123</sup> for selecting the models of normal, confined, drift-containing, and anomalous diffusion for multiple sets of biological SPT data. Below, we apply these model-

ranking and parameter-estimation algorithms to experimental data of tracer diffusion in mucin hydrogels<sup>19,20</sup>. We overview the features of anomalous, non-ergodic, and non-Gaussian diffusion of tracers in mucin gels in Sec. III. We refer to Ref.<sup>49</sup> for the detailed description of the DD model, underlying equations, and computational algorithm.

### III. RECENT EXPERIMENTAL INSIGHTS

#### A. Mucin gels: structure and diffusive properties

Here, we use the data of Ref.<sup>19</sup> for diffusion of  $\mu\text{m}$ -sized beads in mucin MUC5AC gels ("spider webs"<sup>17</sup>, Fig. 1b) at rather *dilute* concentrations of 1 wt % mucin and varying pH conditions. Variations in the pH level mimic the natural variability of conditions encountered for mucus films in the body, see Fig. 1a. For specific details on gel preparation, experimental setup, measurement procedure, data-acquisition protocols—including the removal of centre-of-mass motion for each tracer<sup>20</sup> by a drift-correction algorithm—we refer the reader here to the original studies<sup>19,20</sup>. We apply the Bayesian approach with the nested-sampling algorithm for BM, FBM, and DD, as developed in Refs.<sup>49,63</sup>, to the data<sup>19</sup> to quantify the most statistically appropriate models for each trajectory. We evaluate additional statistical quantifiers, to complement the analysis of Refs.<sup>19,20</sup>.

As mentioned in Sec. IB, extremely long mucin polymers form hydrogel-like networks stabilised by reversible hydrophobic interactions and repulsive electrostatic forces between the sugar side-chains<sup>14,19,20,30</sup>. The microstructure of these biogels alters with solution acidity: for instance, upon lowering the pH from pH=7 to pH=2 the macrorheological measurements<sup>19</sup> revealed a dramatic,  $\gtrsim 100$  times, increase in their viscoelastic moduli (at pH=2 the gel is more solid-like and mucin chains become progressively unfolded<sup>20</sup>). This solid-like response is likely due to less dissociation and a more cross-linked network. At higher pH values (pH=7), mucin chains repel one another due to non-compensated negative charges, resulting in a more liquid-like gel with smaller viscoelastic moduli<sup>19,174</sup>.

To quantify biochemical changes, the strength of mucin interactions, and the network permeability at different pH levels and salt conditions, a detailed analysis of TAMSDs of carboxylated  $\mu\text{m}$ -sized spheres—negatively charged at pH=7 and less charged at pH=2<sup>20</sup>—was performed<sup>19,20</sup>. Such tracers stick less to mucins<sup>39</sup> and yield diffusion least obstructed by interactions. All trajectories analysed below were taken on mucin samples<sup>19</sup> with a square cross-section of (0.9 mm)  $\times$  (0.9 mm) and length of 20 mm, put inside 3D capillary tubes (see Sec. 2.3.1 of Ref.<sup>20</sup>). Reference<sup>20</sup> also contains a detailed description of further details of the SPT apparatus, estimation of static and dynamic errors<sup>129</sup> of the measurements, data-pretreatment methods, etc.

Three-dimensional tracer motion effectively tracked in a two-dimensional focal plane of the microscope and the trajectories are limited to  $N_p = 300$  points<sup>19</sup> (with camera framerate of  $\approx 30$  fps and exposure time of  $\approx 33$  msec). The trace-length is  $T = 10$  sec. The pre-set values of  $N_p$  and  $T$  can affect the results of ensemble averaging and the accuracy of further estimations, see Sec. V and Refs.<sup>107,130</sup>. Note that with a  $20\times$  lens one usually focuses on 10-12 distinct particle  $z$ -planes when working with well mixed mucin gels. The uncertainty in determining tracer positions in the SPT experiments<sup>19,20</sup> was  $\sim 0.3 \dots 1$  pixel, with  $1 \mu\text{m} = 1 \text{ pixel} \times (13/20)$ . The estimate for confidently defined tracer (static) positions<sup>19</sup> is based on an agarose immobilisation assay, with the static uncertainty of  $|\Delta x| \lesssim 0.01 \mu\text{m}$ , Fig. 2.3.2 of Ref.<sup>20</sup>.

For lag times from  $\Delta \approx 33$  msec (experimental time-resolution) to  $\Delta \approx 4$  sec no dramatic or systematic changes in the scaling exponent of the TAMSD was detected upon changing pH from pH=7 to pH=4, and, eventually, to pH=2. Namely, with no added salt ( $n_0 = 0$ )—see Refs.<sup>19,20</sup> for the exact buffer conditions—the TAMSD exponent at short lag times decreases from  $\beta_{\text{pH}=7} \approx 0.85$  to  $\beta_{\text{pH}=4} \approx 0.61$ , while then it increases again to  $\beta_{\text{pH}=2} \approx 0.92$ <sup>19,20</sup>. The tracer mobility at pH=2 was, however, the highest. Figure 2a shows representative tracer trajectories recorded<sup>19</sup> at pH=2 (see also the video files). The tracer beads are less negatively charged (of even positively charged) at pH=2, as compared to pH=7<sup>19,20</sup>, that also affects their mobility. This may complicate the quantification of pH effects, as discussed in Refs.<sup>19,20,175</sup>

The PDFs of tracer displacements after a fixed time  $t = 0.1$  sec were shown<sup>19</sup> to be roughly Gaussian, except at pH=2, Fig. 2b. At pH=2 for displacements for a sub-population of tracers is close to exponential, an possible indicator of a DD models<sup>67,100,101,109</sup>. We show in Sec. IV A, however, that the DD model is only rarely realised for this data<sup>19</sup>. Note also that pronouncedly broader-than-Gaussian PDFs at pH=2 are responsible for overall *larger* magnitudes of TAMSDs at these conditions<sup>19,20</sup>, Fig. 3. This heterogeneity of magnitudes of individual TAMSDs renders the MSD  $\langle x^2(\Delta) \rangle$ , see the inset of Fig. 3, to be much less informative quantifier of diffusion, as compared to the set of  $\overline{\delta_i^2}(\Delta)$ .

#### B. Population splitting and non-ergodicity

The data<sup>19</sup> at pH=2 revealed comparatively high values of the heterogeneity parameter, HR (equivalent to the EB parameter (4)). This increase (see also the discussion below) was proposed<sup>19</sup> to be caused by a strongly heterogeneous structure of the mucin network, with polymer-rich and polymer-poor regions emerging at pH=2 (Fig. 1b), as compared to a rather homogeneous network at pH=7. Mucin-rich and mucin-poor regions can, correspondingly, hamper and promote tracer diffusion (see Fig. 1b), resulting in subpopulations of slow and fast

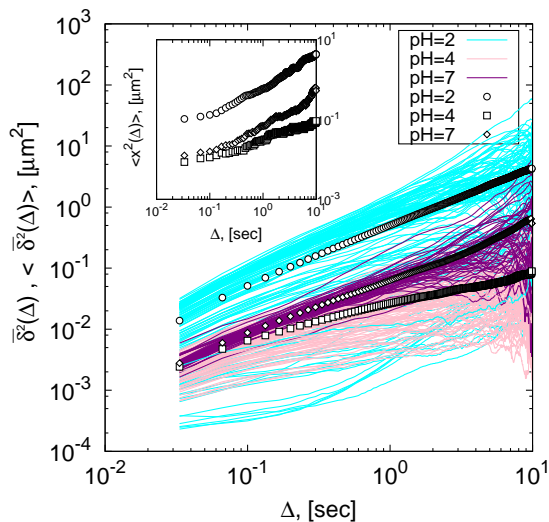


FIG. 3: Spread of individual TAMSD trajectories (2) for the data of Ref.<sup>19</sup> with  $T = 10$  sec. Different colours denote varying pH conditions. At pH=2 the data set of experiment #2 of Ref.<sup>19</sup> was used, see also Fig. 5. The inset presents the ensemble-averaged MSDs, for the purpose of comparison.

(possibly, weakly *superdiffusive*) tracers.<sup>176</sup> Network heterogeneities at pH=2 were studied in Ref.<sup>20</sup>.

Therefore, one can split the trajectories into a slow subpopulation with exponential and a fast subpopulation with Gaussian displacement distributions<sup>19</sup>. This provided a physical rationale for some features of the PDFs of tracer displacements in mucin gels<sup>19,20</sup>. The probability of displacements  $\Delta x$  after a time-interval  $t$  was proposed to obey<sup>19</sup>

$$P_{\text{fit}}(\Delta x, t) = \frac{A \exp\left(-\frac{(\Delta x)^2}{2\sigma^2(t)}\right)}{\sqrt{2\pi\sigma^2(t)}} + \frac{(1-A) \exp\left(-\frac{|\Delta x|}{\lambda(t)}\right)}{\sqrt{4\lambda^2(t)}}. \quad (10)$$

The magnitude of TAMSDs for these subpopulations at pH=2, at short lag times grows with the exponents  $\beta \approx 0.95$  and  $\beta \approx 0.75$ <sup>19</sup>, respectively. The spread of  $\overline{\delta_i^2}(\Delta)$  was shown to be considerably larger for the exponential subgroup<sup>19,20</sup>, reflected also in the magnitudes of the non-Gaussianity parameter (6), as examined in Refs.<sup>19,20</sup>. Importantly, in Eq. (10) the fraction  $A(t)$  of tracers diffusing in a Gaussian-like way—as determined from the short-time behaviour of  $\overline{\delta_i^2}$ <sup>19</sup>—stays nearly *constant* with time:  $A(t) \approx \text{const}$  within the duration of experiments that validates the division method (10). Moreover, in Eq. (10) the typical length-scales for Gaussian and exponential subpopulations of the tracers were shown<sup>19</sup> to scale as  $\sqrt{2\sigma^2(t)} \sim t^{0.48}$  and  $\sqrt{4\lambda^2(t)} \sim t^{0.39}$ , respectively. These values of the scaling exponent of the width are consistent with those for the TAMSD growth (2) for respective subpopulations, making this description self-consistent.<sup>177</sup>

For the mucin gels at pH=2 the conclusion<sup>19</sup> was

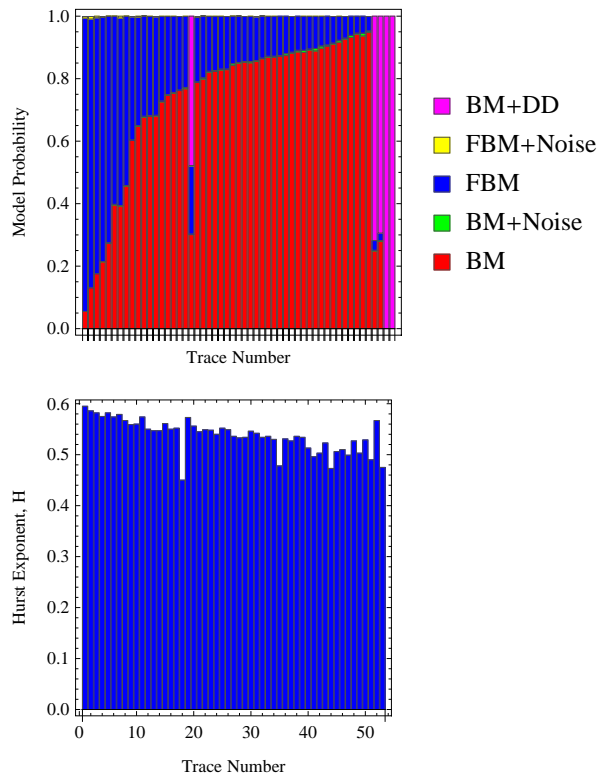


FIG. 4: Results of model comparison from the Bayesian analysis using nested sampling and Hurst exponent distributions for diffusion of tracers in mucin gels at pH=7, obtained for the data set of Ref.<sup>19</sup>. The trajectories here are ordered according to decreasing probabilities of the FBM model (in the top graph, from left to right). The respective exponents  $H_i = \beta_i/2$  are shown in the bottom graph.

that—due to their inherent heterogeneities—“Gaussian-like” particles sample rather mucin-poor regions, being minimally-affected by its structure (Fig. 1b). In contrast, “exponential” tracers are probing more mucin-rich regions, with different values of network stiffness<sup>19,20</sup>, leading to “confined diffusion”, Fig. 1b. The “Gaussian” tracers, thus, produce a bell-shaped Gaussian PDFs of displacements, whereas “exponential” tracers are responsible for non-Gaussian features of  $P(x, t)$ , particularly pronounced at pH=2<sup>19,178</sup>. As outlined in Fig. 2b, after a diffusion time  $t = 0.1$  sec, the displacements of highly diffusive particles have broader “tails”, as compared to those of strongly confined ones<sup>19,179</sup>.

## IV. MAIN RESULTS OF THE DATA ANALYSIS

### A. Bayesian analysis and model-prediction results

We performed the maximum-likelihood Bayesian analysis with the nested-sampling algorithm for the data sets of tracer diffusion in mucin hydrogels<sup>19</sup> in the absence of salt,  $n_0 = 0$ <sup>20</sup>. For pH=7 the model of BM appears to

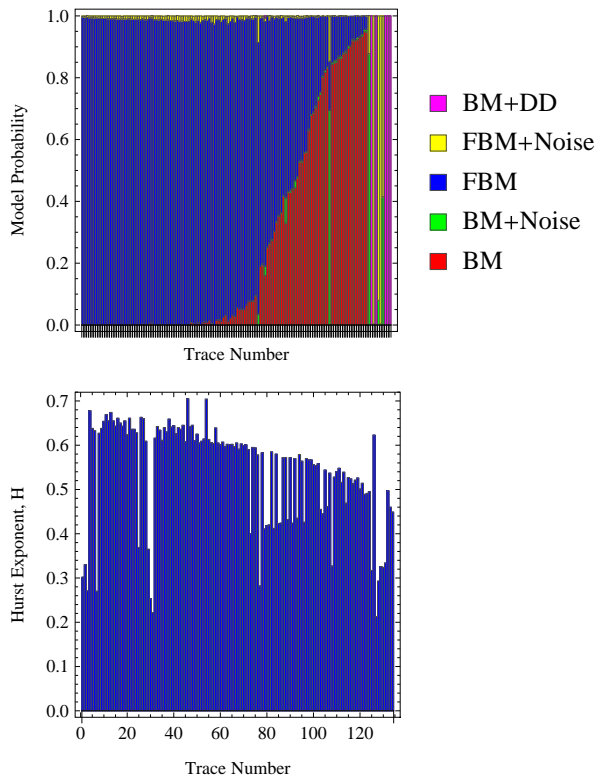


FIG. 5: The same as in Fig. 4 but at pH=2 (the data set of experiment #2 of Ref.<sup>19</sup> with  $N = 134$  traces is used here).

dominate the single-trajectory data, see Fig. 4. At these conditions for FBM-dominated trajectories the Hurst exponent progressively decreases from  $H \approx 0.6$  to  $H \approx 0.5$  as the model preference is changing from FBM to BM for the set of trajectories analysed. Overall, at these conditions the model of Fickian diffusion dominates the dynamics in mucin networks, whereas several trajectories do favour the DD model of as the most statistically preferred one, Fig. 4.

For the data at pH=4 we observe that FBM dominates the model-prediction results, with considerably *more subdiffusive* exponents  $H$ , Fig. A3. This fact is consistent with the evolution of TAMSDs upon a transition from pH=7 to pH=4 (Fig. 4a in Ref.<sup>19</sup>). The Hurst index for trajectories fitted with the FBM model at pH=4—when ordered from least subdiffusive to most diffusive—grows from  $H \approx 0.3$  to  $H \approx 0.5$  as we progress from FBM- to BM-favouring trajectories. This is a physically meaningful behaviour: scaling exponents increase as the FBM model gets replaced by BM with a linear MSD, i.e., with  $H = 0.5$  in Eq. (1). These trends for  $H$  are statistically significant, Fig. A3. For the data set at pH=4 almost no trajectories were found consistent with the DD model.

Finally, for the data set at pH=2 we find more interesting behaviour and a very heterogeneous picture, as mentioned in Refs.<sup>19,20</sup>. This heterogeneity can be caused by size variations of typical hydrogel structures which hamper tracer diffusion and also arise due to batch-to-batch

variation of the purified mucin. Moreover, some variations for different data sets acquired at this pH value were found, compare Figs. A4, 5, and A5 containing  $N = 64, 134,$  and  $334$  time series, respectively (obtained from *different* experiments in Ref.<sup>19</sup>, (#1, #2, and #3)). Although the conditions of these measurements were kept the same, some *ageing effects* may be present<sup>30</sup>, although subsequent study by the authors of Refs.<sup>19,20</sup> did not reveal strong ageing at pH=2 (unpublished). The ageing times in the course of sample preparation were, however, not recorded in Ref.<sup>19</sup>, making statistical analyses of ageing impossible for these data (not shown). Although we do find that FBM-based diffusion dominates the data at pH=2, the exponents  $H_i$  vary strongly from trace to trace at these conditions (heterogeneous medium).<sup>180</sup>

Additionally, the variations of scaling exponents reveal the existence of *two subpopulations* of tracers in the data set at pH=2, Fig. 5. In a slower subpopulation the Hurst exponent varies in the range  $H \approx 0.3 \dots 0.5$ , while in a more diffusive subpopulation  $H \approx 0.5 \dots 0.65$ . The first subpopulation corresponds to subdiffusion with a TAMSD exponent of  $\beta \approx 0.6 \dots 1$ , while the second subgroup describes superdiffusion with  $\beta \approx 1 \dots 1.3$ . We mention here that superdiffusion was also observed for worm-like micellar solutions<sup>134</sup>. Note that for even larger number of trajectories at pH=2, as in experiment #3 of Ref.<sup>19</sup>, one can distinguish even *three subpopulations* of tracers, featuring Hurst exponents within *three* distinct ranges, see Fig. A5.

We emphasise that the models of BM and FBM containing a Gaussian noise of certain strength have low model probabilities, in comparison to their pure analogues, see Figs. 4, 5, and A5. These "noisy" models become penalised in our Bayesian model-prediction results due to Occam's razor. This results mainly from the fact that the uniform prior used for the noise strength (see Apps. A and B for details), does not increase the maximum-likelihood value of "noisy" models significantly enough in order to compensate the "negative" effect for these models stemming from an additional model parameter, see Refs.<sup>51,53</sup>.

As the top panel of Fig. 5 shows—as the FBM model gets replaced by BM as the most appropriate model of tracer diffusion<sup>19,20</sup>—the respective Hurst exponents in each subpopulation approach  $H \approx 0.5$ , as expected. For experiment #2 at pH=2, we observe that only half-a-dozen of trajectories is consistent with the DD model, Fig. 5. This small number is unlikely to result in an exponential—rather than in a Gaussian—PDF of displacements observed for the "exponential" subpopulation of tracers<sup>19,181,182</sup>. We propose that at pH=2 the diffusive medium is most heterogeneous (Fig. 1b) that gives rise to broad distributions of generalised diffusion coefficients and scaling exponents (Fig. 6). Therefore, it is rather ensemble averaging over all trajectories subject to certain distributions  $p(K_\beta)$  and  $p(\beta)$  that yields non-Gaussian dynamics (on, possibly, multiple timescales).

## B. Spread of TAMSD trajectories

To further quantify the dynamics of tracers in mucin gels<sup>19,20</sup>, we employ additional statistical measures<sup>66,74,91,107</sup> including the spread of individual TAMSDs presented in Fig. 3. As mentioned in Refs.<sup>19,20</sup>, we find that the spread is minimal at pH=7 and maximal for strongly heterogeneous diffusion at pH=2. Moreover, to support the trends found from the Bayesian analysis, in Fig. 6 we present the results of the direct power-law fit of  $\overline{\delta_i^2(\Delta)}$  of tracers in mucin gels. We compute the values of the scaling exponent  $\beta_i$  and generalised diffusion coefficient ( $K_{\beta}$ )<sub>*i*</sub> for the *i*th trace from

$$\overline{\delta_i^2(\Delta)} \approx 4(K_{\beta})_i \times \Delta^{\beta_i}. \quad (11)$$

In the SPT experiments<sup>19</sup> the particles are effectively tracked in *two dimensions* (leading to the factor of four in Eq. (11)). The number of points in the initial range of trajectories used for the fit (11) is  $N_{\text{fit}} = 10$ . Choosing a shorter initial fragments would slightly increase  $\beta_i$  values for TAMSD fits, making their agreement with the Bayesian results of Fig. 6 even closer.<sup>183</sup>

Fitting  $N_{\text{fit}} = 10$  points for the data at pH = {2, 4, 7} results in MSD exponents

$$\alpha \approx \{0.46, 0.28, 0.36\} \quad (12)$$

and mean TAMSD exponents

$$\langle \beta \rangle \approx \{1.09, 0.75, 0.94\}, \quad (13)$$

see Fig. 3. Some discrepancies of the obtained  $\beta$  values (13) from those reported in Ref.<sup>19</sup> can be, e.g., due to a different number of fitting points used,  $N_{\text{fit}}$ . A favourable overall comparison of respective anomalous exponents and generalised diffusivities, as shown in Figs. 6a and 6b, makes us confident in the robustness and accuracy of the employed Bayesian algorithm with nested sampling. Significantly different magnitudes and scaling exponents of the MSDs and mean TAMSDs for respective pH conditions (see Eqs. (12) and (13)) indicate *weak ergodicity breaking*, see Sec. IV D.

At all pH values, the MSDs grow with time slower than the TAMSDs. Note that these results involve ensemble averaging with trajectory-specific exponent and diffusivities. Therefore, the discrepancy between  $\alpha$  and  $\langle \beta \rangle$  can still allow individual time series to be governed by an *ergodic* process (BM, FBM). Moreover, as outlined in Ref.<sup>19</sup>, on the level of individual trajectories the tracer displacements can be nearly Gaussian, while for the whole ensemble of particles the displacements at the same conditions are distinctly non-Gaussian (see also Figs. A11, A12, and A13).

Figure 6a shows that the spread of scaling exponents for diffusion at pH=2 is maximal (the most-heterogeneous medium), while at pH=7 the spread is limited. The pronounced spread of  $\overline{\delta_i^2(\Delta)}$  is consis-

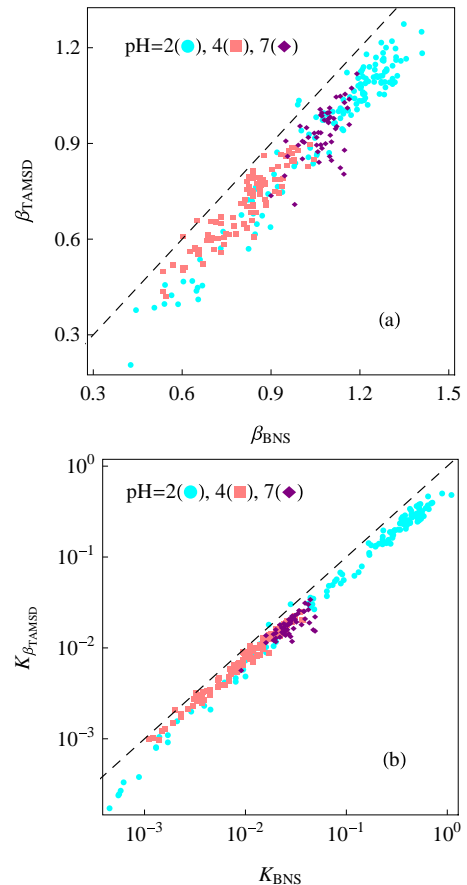


FIG. 6: Correlations of the scaling exponents (a) and generalised diffusion coefficients (b), as obtained from the Bayesian nested-sampling analysis (the subscript "BNS") and via direct power-law fit of  $\overline{\delta_i^2(\Delta)}$  by Eq. (11). The results for different pH values are in the same colours as in Fig. 3; the data set of experiment #2 is used at pH=2. The dashed lines are the diagonals: the respective quantities are equal there. The Pearson correlation coefficients for the data sets of  $\{\beta_{\text{TAMSD}}, \beta_{\text{BNS}}\}$  and  $\{K_{\beta_{\text{TAMSD}}}, K_{\text{BNS}}\}$  are, respectively,  $r \approx \{0.97, 0.93, 0.61\}$  and  $r \approx \{0.98, 0.98, 0.68\}$ , computed for the set of pH values pH = {2, 4, 7}, respectively.

tent with the available evidences and data<sup>11,17,144,145</sup>. This reflects heterogeneities of the meshwork of entangled mucins: some tracers diffuse nearly freely, while others are strongly impeded in their spreading (see the division into "Gaussian" and "exponential" tracers<sup>19</sup> and Fig. 1b). We also mention that, particularly at pH=2, the fraction of *superdiffusive* trajectories is comparatively large, see Fig. 6a, corroborating with the Bayesian results of Fig. 5. The set with  $N = 134$  is used in Fig. 6 at pH=2. For this set, we revealed positive correlations between the errors in determining the Bayesian exponents  $\Delta\beta_{\text{BNS}}$  and the values of  $\beta_{\text{BNS}}$  themselves, Fig. A6.<sup>184</sup>

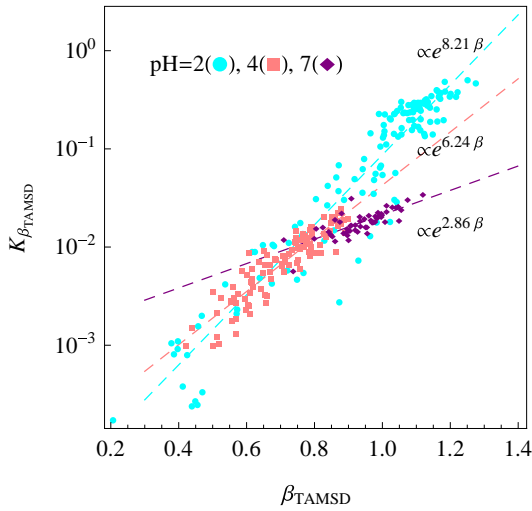


FIG. 7: Correlation of scaling exponents and diffusion coefficients obtained via fitting  $\overline{\delta_i^2(\Delta)}$  with Eq. (11) at the start of the recorded time series. The dashed lines are the best linear fits of  $\log(K_\beta)$  versus  $\beta$ .

### C. Positive $K_\beta$ - $\beta$ correlations

Another characteristic feature of tracer diffusion in mucin gels<sup>19,20</sup> is a pronounced *positive correlation* of anomalous scaling exponents  $\beta$  and generalised diffusion coefficients  $K_\beta$  for individual trajectories. We find these correlations for all pH values, Fig. 7. This is a new feature as compared to the previous analyses<sup>19,20</sup>. We fit these correlations with

$$K_\beta(\beta) \sim \exp(c_1\beta + c_2), \quad (14)$$

where  $c_{1,2}$  are the parameters, shown in Fig. 7 as the dashed lines (different colours for different pH values). The Pearson's correlation coefficients for the sets  $\{K_{\beta_{\text{TAMSD}}}, \beta_{\text{TAMSD}}\}$  are  $r \approx \{0.86, 0.85, 0.76\}$ , respectively, for  $\text{pH} = \{2, 4, 7\}$ . Moreover, the data set at  $\text{pH}=2$  reveals *two distinct regions* in the phase-space with large and small exponents of the  $\overline{\delta_i^2(\Delta)}$  growth,  $(\beta_{\text{TAMSD}})_i$ . This illustrates "population splitting" reported in Ref.<sup>19</sup> based on criteria of splitting the trajectories for the PDFs of individual tracers.<sup>185</sup>

### D. Ergodicity breaking parameter

The inset of Fig. 3 reveals some *discrepancies* between the MSDs and mean TAMSDs, particularly for the short-time growth of  $\langle x^2(\Delta) \rangle$  and  $\langle \overline{\delta^2(\Delta)} \rangle$  at  $\text{pH}=2$ . The degree of irreproducibility of individual TAMSDs for tracer diffusion in mucin gels is quantified in terms of the ergodicity breaking parameter (4). Figure 8 illustrates the evolution of EB for different pH values. Larger spread of  $\overline{\delta_i^2}$  at  $\text{pH}=2$  is consistent with larger EB for this pH,

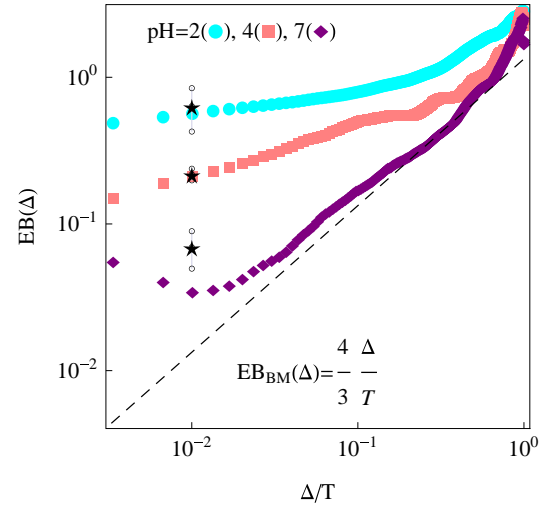


FIG. 8: EB parameter (4) for tracer diffusion in mucin gels at different pH values<sup>19</sup> (for the data of Fig. 3). The BM asymptote (15) is the dashed line; compare also to the DD results in Fig. A1. The results of Ref.<sup>19</sup> for the HR parameter are the star symbols (with the error bars), Sec. IV D).

and also with the EB value not decaying to zero as a power-law of  $(\Delta/T)$  at short lag times. Note that in Refs.<sup>19,20</sup> at lag time  $\Delta = 0.1$  sec, the heterogeneity parameter was computed to be  $\text{HR} \approx 0.07 \pm 0.02$  at  $\text{pH}=7$ ,  $\text{HR} \approx 0.22 \pm 0.02$  at  $\text{pH}=4$ , and  $\text{HR} \approx 0.64 \pm 0.21$  at  $\text{pH}=2$ , see Fig. 8.

Note that the EB parameter was evaluated for a number of stochastic processes (normal and anomalous), including regular BM<sup>86,148</sup>, FBM<sup>86,149</sup>, continuous-time random walks<sup>73,74,150</sup>, and heterogeneous diffusion processes<sup>127,151</sup>, the OU process<sup>114</sup>, and scaled Brownian motion<sup>82,152,153</sup>. Note also that for FBM with MSD exponents in the range  $0 < \alpha < 3/2$  for short lag times the EB parameter scales as  $\text{EB}(\Delta) \sim \Delta/T$ , while it decays at  $\Delta/T \rightarrow 0$  slower than linear for the range  $2 > \alpha > 3/2$ , namely  $\text{EB}(\Delta) \sim (\Delta/T)^{4-2\alpha}$ <sup>149</sup>.

We find that at  $\text{pH}=7$ <sup>19,20</sup> for intermediate lag times the EB parameter is fairly close to the BM limit<sup>66,86,114</sup>,

$$\text{EB}_{\text{BM}}(\Delta) = 4\Delta/(3T). \quad (15)$$

This is corroborated by a limited spread of TAMSDs and the value of the scaling exponent (13) at  $\text{pH}=7$ , see Fig. 7, as well as by small non-Gaussianity parameters found for these conditions in Refs.<sup>19,20</sup>. We mention that the linear  $\text{EB}(\Delta/T)$ -dependence is no longer valid at  $\text{pH}=4$ , where the scaling becomes *sublinear*, Fig. 8. For short lag times it can be approximated by

$$\text{EB}(\Delta/T) \sim (\Delta/T)^\epsilon, \quad \text{with } \epsilon < 1. \quad (16)$$

The deviation from the BM law (15) is especially pronounced at  $\text{pH}=2$  when almost a *plateau region* emerges in the  $\text{EB}(\Delta)$  evolution at short  $\Delta$ .

This is reminiscent of the EB behaviour for continuous-

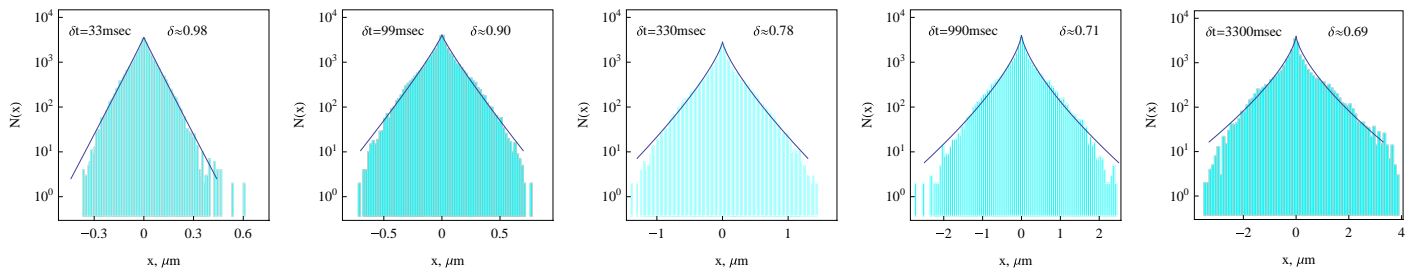


FIG. 9: Non-Gaussian distributions of displacements for tracers diffusing in mucin gels at pH=2 (shown as counts,  $N(x)$ ). The results are plotted for varying time shifts from the start of the trajectories,  $\delta t$ . The data sets of Ref.<sup>19</sup> are used. The best-fit exponents  $\delta$  in the compressed Gaussian distribution (18) are given in each panel.

time random walks<sup>66,73,74,149,150,154</sup> with the MSD exponent  $\alpha$ , where at  $\Delta/T \ll 1$  it was predicted that

$$EB(\Delta/T \rightarrow 0) = 2\Gamma(1 + \alpha)^2/\Gamma(1 + 2\alpha) - 1, \quad (17)$$

where  $\Gamma(\cdot)$  is the Gamma function. This fact also corroborates with the pronounced spread of TAMSD realisations at short lag times for the data set at pH=2, see Fig. 3. The strongly heterogeneous nature of the polymer network realised at pH=2 conditions, Fig. 1b, favours widely distributed particle-network trapping conditions (in terms of energetic barriers to escape network-imposed confinement or caging). This, in turn, produces strongly distributed effective diffusivities of the tracers and strongly spread magnitudes of individual TAMSDs. The behaviour of EB at pH=2 for different sets (with  $N = 64, 134, 334$  traces<sup>19</sup>) is shown in Fig. A8a.<sup>186 187</sup>

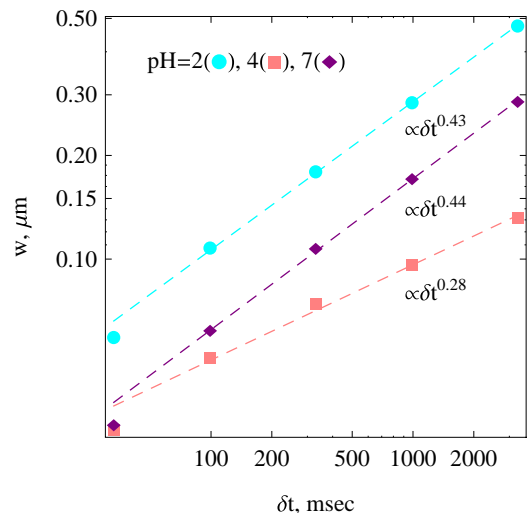


FIG. 10: Scaling of the width of PDFs of tracers diffusing in mucin gels<sup>19,20</sup>. The exponents  $\gamma$  are evaluated from Eq. (19) at different pH values, as indicated in the plot.

We now study the mean TAMSD magnitudes from Fig. 3 for systematically varying number of points in the trajectory, for  $T = 10, 30, 100, 300$  points. We rescale the data using the relation  $\langle \delta^2(\Delta) \rangle \simeq \Delta/T^{1-\alpha}$ , characteristic for subdiffusive continuous-time random walks<sup>66,73,74</sup>. We observe that for pH=4 and pH=7 practically *no dependence* on the trace length  $T$  exists, Fig. A8b. Here, the shortest lag time of  $\Delta = 1$  step and the respective MSD scaling exponents (12) were used in the analysis. Therefore, we can *rule out* continuous-time random walk as another possible model of diffusion. This is also consistent with a rather limited spread of TAMSDs at these conditions, Fig. 3. At pH=2, however, there is a remaining but weak  $T$ -dependence in the  $\langle \delta^2(\Delta, T) \rangle$  data. Although the spread of TAMSDs is indeed the largest at pH=2, the observed dependence  $\langle \delta^2(\Delta = 1, T) \rangle$  is too weak for the continuous-time random walk scenario to be considered as an alternative model realised for tracer diffusion in mucin gels.

### E. Non-Gaussian PDFs of tracers

The distributions of displacements of the tracers, as monitored in the experiments<sup>19,20</sup>, are presented in Figs. 9, A9, and A10 (respectively, for pH=2, 4, and 7, see also the supplementary video files). The analysis below is performed only for the  $x$ -component of displacements *of all the tracers* (the  $y$ -behaviour is identical, due to isotropy of the system). We fitted the observed PDFs with a stretched or compressed exponential function, for logarithmically sampled time intervals from the start of diffusion,  $\delta t$ . Particularly at pH=2 the displacements were found pronouncedly non-Gaussian, consistent with previous conclusions<sup>19,20</sup>. For pH=4 and, particularly, for pH=7, the PDF functions were closer to the Gaussian shape, still revealing some larger than Gaussian displacements of the tracers, Fig. A10.

We fit the step-size distributions with a two-parameter function (width and exponent) in **Wolfram**

Mathematica,

$$P(x, \delta t) \sim \exp(-(x/w)^\delta). \quad (18)$$

We find that the fitted exponents  $\delta$  drop continuously for longer time intervals  $\delta t$ , see Figs. 9, A9, A10. Namely, for the time-shift increasing from  $\delta t = 33$  to 3300 msec the exponent  $\delta$  in (18) drops from  $\delta \approx 0.98$  to  $\approx 0.69$  and from  $\delta \approx 1.63$  to  $\sim 1.40$ , respectively, for pH=2 and pH=4 sets. This indicates that the tracers are progressively *slowed down* at later stages of diffusion (longer  $\delta t$  times). For pH=7, in contrast, the PDF exponents  $\delta$  stay nearly constant with the time shift, assuming a large value of  $\delta \approx 1.60$  that is close to  $\delta = 2$  for a Gaussian<sup>66,79</sup>. The PDFs for all the tracers at pH={2, 4, 7}<sup>19</sup> are shown in Figs. 9, A9, and A10, respectively.

The width of these stretched or compressed exponential distributions are found to grow with the time shift, Figs. 9 and 10. The exponents  $\gamma$  of a power law for scaling of the PDF widths,

$$w^2(\delta t) \sim (\delta t)^\gamma, \quad (19)$$

found from our analysis are close to the exponents of the mean TAMSDs  $\langle \beta \rangle$  at respective pH conditions, compare Figs. 3 and 10. This supports our analysis for the scaling law for the growth of  $\langle \delta^2(\Delta) \rangle$  (see Eqs. (11) and (13)) and of the widths of the PDFs (see Eq. (19)), as intuitively expected.<sup>188</sup>

In Figs. A11, A12, and A13 we present the results of fitting of the widths of displacement distributions for *individual* tracers, denoted  $P_i(x, t)$ . This representation is different from fitting the *ensemble* of displacements of all the tracers at a given time shift, as in Figs. 9, A9, and A10. From single-trace fits of Fig. A11 we find that at pH=2 those two traces for which the Bayesian nested-sampling analysis consistently predicts the DD model yield indeed nearly exponential PDFs. Specifically, we find  $\delta \approx 0.90$  and  $\approx 1.01$  for traces #18 and #28 in Fig. A11, respectively.<sup>189</sup> For these trajectories, very small widths of the PDFs are observed,  $w_i$ . Other trajectories favouring the DD model<sup>190</sup> are, however, not close to the exponential PDFs, revealing decay exponents in the range  $\delta \approx 1.75 \dots 1.81$ , see Fig. A11. Therefore, the DD model might not be optimal to rationalise the observed close-to-exponential distributions of displacements for a subpopulation of "exponential" tracers, see Eq. (10).

Overall, at pH=2 the heterogeneity of  $P_i(x, \delta t)$  functions is dramatic, even at the shortest time shift of  $\delta t = 33$  msec. For instance, we detect *large variations* of the scaling exponent  $\delta_i$  and, particularly, of the PDF width  $w_i$  for each trajectory, as illustrated in Fig. A11. The trajectories predicted to favour the DD model correspond to the particles that feature rather *narrow* PDFs of displacements (respectively, small  $w_i$  values).

For tracer diffusion at pH=4<sup>19</sup> we find a substantially smaller spread of scaling exponents  $\delta_i$  in Eq. (18) than at pH=2, with the values in the range  $\delta \approx 1.6 \dots 2.3$ , see

the top panel of Fig. A12. The widths of  $P_i(x, \delta t)$  for individual particles at these conditions are shown in the bottom panel of Fig. A12 (see also the PDF shapes for the whole data set in Fig. A9). At pH=4 we thus detect no trajectories dominated by the DD model.

Lastly, at pH=7 the spread of the PDF widths is even smaller (consistent with fairly reproducible TAMSDs at this pH value, see Fig. 3). The scaling exponents of individual  $P_i(x, \delta t)$  functions for five traces is very close to unity, see the magenta bars in Fig. A13. This, indeed, is realised for the traces consistent with the DD model, with the exponents  $\delta \approx \{1.03, 1.03, 1.03, 0.97, 0.91\}$ . The results of fitting PDFs computed from single trajectories are shown in Fig. A13.

To illustrate the spread of the widths of the fitted stretched Gaussian and compressed exponential distributions, in Fig. A14 we present the histograms of (width)<sup>2</sup>-distributions for PDFs (18) at all pH values<sup>19,20</sup>. In this plot, the trajectories are ordered from larger to smaller values of the PDF widths. We find a rather homogeneous distribution  $p(w^2)$  for pH=7 and somewhat heterogeneous one (with a similar mean) at pH=4. In contrast, at pH=2 the distribution  $p(w^2)$  is *extremely broad*, with considerably larger  $w_i^2$  values on average. This strongly heterogeneous distribution of widths of the PDFs is consistent with a dramatic spread of TAMSDs at pH=2, as seen in Fig. 3.

## F. Displacement autocorrelation function

For the experimental data<sup>19</sup> we compute the displacement autocorrelation function from the radius-vector of diffusing tracers,  $\mathbf{r}(t)$ , as follows<sup>66,74</sup>

$$C_{dt}(t) = (dt)^{-2} \langle [\mathbf{r}(t+dt) - \mathbf{r}(t)] \cdot [\mathbf{r}(dt) - \mathbf{r}(0)] \rangle. \quad (20)$$

This function correlates *particle displacements* at time  $t$  to its displacements at initial time for a finite time shift,  $dt$ .<sup>191</sup> The results for  $dt = 1$  are shown in Fig. 11, where each trajectory is divided into fragments of  $N_{\text{sub}} = 10$  points (the results shown in lighter colours in the plot). Final averaging is performed along each trajectory and over all the traces in the set<sup>19</sup> (the solid symbols connected by thick lines in Fig. 11). We emphasise large statistical uncertainties when  $C_{dt}(t)$  is computed solely for a *one stretch* of a given trajectory.

We observe in Fig. 11 that for a rather subdiffusive set of trajectories at pH=4 the function  $C_{dt=1}(t)$  attains *negative values* after one experimental time step. This behaviour—consistent with FBM-like subdiffusion<sup>66,74</sup>, as our Bayesian single-trajectory analysis also suggests—indicates a certain degree of *antipersistence* in tracer motion. The drop of  $C_{dt=1}(t = 1)$  below zero is not very pronounced at pH=4<sup>19</sup>, but the effect is way larger than the *error bars* computed, Fig. 11.

For tracer diffusion at pH=2 and 7, on the contrary, the displacement autocorrelation function *does not* drop

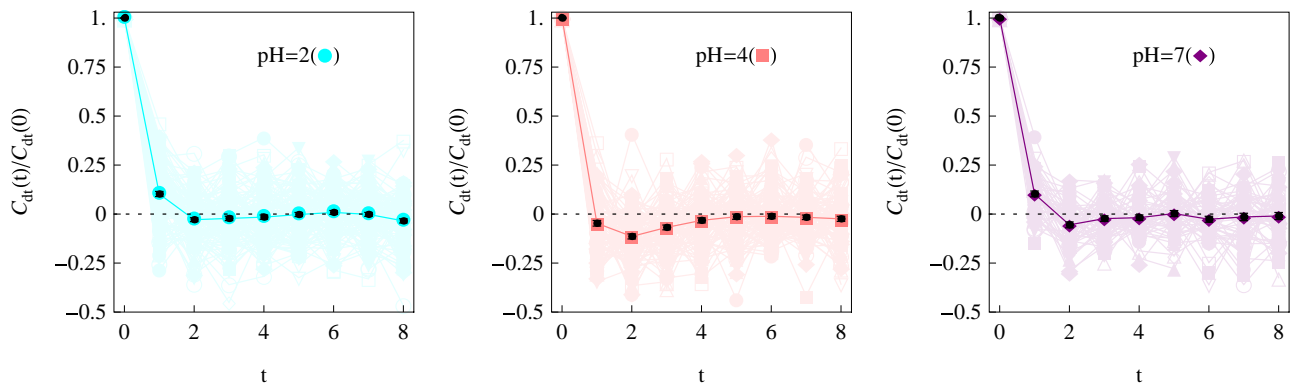


FIG. 11: Displacement autocorrelation function—defined in Eq. (20) and normalised to its value at  $t = 0$ —computed for tracer diffusion in mucin gels<sup>19</sup> at the pH values as indicated. The time shift here is one experimental frame,  $\delta t = 1$  or  $dt \approx 0.033$  sec. The results of double averaging—namely, for different fragments along the trajectories and among different trajectories—are the solid symbols. The error bars are rather small (the black symbols). The colours are the same as in Fig. 3.

measurably below zero (similar as for BM<sup>66,74</sup>). For pH=7 this indicates a "more normal" diffusion, as indeed seen from the behaviour of TAMSDs, see the values of scaling exponents (13) and Refs.<sup>19,20</sup>. We note that at pH=2 a dramatic scatter of TAMSD realisations, see Fig. 3, appears not to cause significant deviations in  $C_{dt}(t)$  from the standard BM-like shape<sup>66,74,158</sup>. The behaviour of  $C_{dt}(t)$  for longer time shifts  $dt$ , shown in Fig. A15, supports these trends. Namely, the most subdiffusive behaviour is indeed realised at pH=4, as follows from the most negative values of  $C_{dt}(t = dt)$  drop found in this situation.

## V. DISCUSSION AND CONCLUSIONS

Understanding the transport and diffusion mechanisms of natural pathogens and artificial tracers in native mucus and reconstituted mucin hydrogels presents a number of challenges, both for SPT measurements, experimental physical chemistry in general, and for theoretical data-analysis of these polymer-based soft-matter systems. The data analysis—based on a number of statistical quantifiers and Bayesian model-ranking approach with the nested-sampling algorithm—is our main focus here.

### A. Main results on tracer diffusion in mucin gels

Here, the central results of our analysis of SPT-data on diffusion of  $\mu\text{m}$ -sized tracers in reconstituted mucin hydrogels<sup>19,20</sup> are summarised. Thermally agitated motion of polymers in these gels governs their structural dynamics<sup>45</sup> and plays a crucial role in controlling transport of tracers and pathogens<sup>13,17,18,21,26,39,40</sup>. We quantified this behaviour using a number of standard statistical quantifiers: namely, the magnitude, spread, and scal-

ing exponents of TAMSDs, non-Gaussian step-size distributions, scaling of widths of the PDFs, the ergodicity breaking parameter, and displacement autocorrelations. We thereby complement the analysis of the same data performed in Ref.<sup>19</sup>, offering a number of decisive statistical features helping a better understanding of this system.

Specifically, we confirmed the largest spread of TAMSDs at pH=2, despite a more subdiffusive behaviour at pH=4, in agreement with previous conclusions<sup>19,20</sup>. Moreover, we unveiled strongly positive correlations between the scaling exponents and diffusion coefficients for individual trajectories. We concluded that tracer diffusion at pH=2 is most heterogeneous and most non-ergodic, based on comparison of  $\text{EB}(\Delta)$  variation at different pH values. We confirmed that SPT data at pH=2 yield the most non-Gaussian PDFs, as compared to pH=4 and 7 (which also decays faster than a Gaussian). The fit of the PDFs for individual tracers,  $P_i(x, t)$ , yielded different exponents  $\delta$  and widths  $w$ , indicating a strongly heterogeneous environment of mucin gels for the tracers at pH=2<sup>19,20,192</sup>.

The main novelty of the current analysis was on applying the Bayesian approach of multiple-hypothesis testing using the nested-sampling algorithm developed by us recently<sup>49,63</sup> for a number of competing ergodic and weakly non-ergodic processes featuring anomalous diffusion—to real experimental data. We examined the SPT data sets of tracer diffusion in mucin gels<sup>19,20</sup>, an example of a disordered polymer-based system with pH-sensitive and ageing behaviours. We discovered that tracer spreading in these gels—on the level of individual trajectories—is dominated by BM and FBM, and only rarely the DD model<sup>49,67</sup> is realised. We remind here that BM/FBM feature Gaussian PDFs<sup>66,74,86</sup>, while the DD model implies an exponential step-length distribution for each trace<sup>63,67,89,100</sup>. Therefore, we propose that

the observed<sup>19,20</sup> non-Gaussian ensemble-averaged distributions of displacements of the tracers are likely due to a *superposition* of Gaussian single-particle PDFs with certain ensemble-specific  $p(K_\beta)$  and  $p(\beta)$  distributions reflecting the relevant properties of the medium.

We also quantified the correlations of the generalised diffusion coefficients and the anomalous scaling exponents of the TAMSDs. This novel, single-trajectory based analysis received some in-depth attention only fairly recently<sup>107,130</sup>. The form of  $K_\beta - \beta$  correlations delivers additional helpful information to decode the nature of the underlying stochastic process and to propose the best physical model of the tracer diffusion. We also confirmed that the values of the scaling exponents for the growth of the mean TAMSDs and for the width of the ensemble-averaged distributions of displacements of the tracers in mucin gels are mutually consistent. This makes the respective laws of anomalous diffusion universal on the timescale of the SPT experiments<sup>19,20</sup>. One more novel measure of the current analysis, as compared that of Refs.<sup>19,20</sup>, is the displacement autocorrelation function,  $C_{dt}(t)$ . The behaviour of the short-time dips of this function appears consistent with the FBM model (proposed also from the single-trajectory Bayesian analysis), including the most subdiffusive behaviour observed at pH=4.

## B. Results of other studies of mucin diffusion

We mention here the results of the likelihood-based analysis and model-comparison tests for two-dimensional data on tracer diffusion in sputum mucus<sup>27</sup> conducted in Ref.<sup>23</sup> (for the 60-fps-data for  $\mu\text{m}$ -sized tracers and 30-sec trajectories). The models of subdiffusive FBM and generalised Langevin equation-based motion were compared<sup>23</sup> via computing the respective Bayes factors. Tracer diffusion at 2.5 and 5.0 wt % of mucus was shown to have a very *pronounced spread* of trajectories<sup>27</sup>, while dilute solutions with 1 wt % revealed nearly BM-like properties<sup>23</sup>. Moreover, the TAMSD exponent was shown to decrease drastically from  $\approx 0.9$  for 1 wt % solutions to  $\approx 0.25$  for 5 wt % of mucus, with a fitted linear decrease  $\langle \beta \rangle \approx 1.1 - 0.17 \times (\text{mucus wt } \%)$ , see Figs. 2B and 4A in Ref.<sup>27</sup>.<sup>193</sup> We refer the reader also to Fig. 2 of Ref.<sup>16</sup> where the diffusivity and anomalous exponent of T4 bacteriophages (particles of  $\approx 200$  nm in size) were measured for varying wt % of mucin. The MSD magnitude was also shown to decrease as wt % of mucin grows<sup>27</sup>. This seemingly beneficial effect for preventing pathogen penetration is, however, apparently out-weighted by other factors (e.g., decreased clearance by cilia beating in the lung)<sup>27</sup>. We refer the reader to Ref.<sup>23</sup> for the discussion of different priors and the significance of multi-parametric diffusion models as well as to Ref.<sup>162</sup> for the Bayesian analysis of FBM-type models with drift. Taken together, the Bayesian analysis of Ref.<sup>23</sup> showed that for diffusive trajectories of micron-

sized tracers in mucin gels the FBM model was outperformed by a model using the generalised Langevin equation with tunable power law relaxation spectra. No models of continuous-type random walk type were analysed in Ref.<sup>23</sup>.

## C. Open questions and future research

*Non-Gaussian PDFs and ensemble heterogeneity.* We obtained from the Bayesian analysis using the nested-sampling algorithm that the models of BM and FBM dominate the results of model ranking for tracer diffusion in mucin gels. The DD model—featuring the exponential displacement distribution<sup>49,67</sup> (7)—is, on the contrary, realised quite rarely for these data. The experimentally observed non-Gaussianity in the PDFs of displacements can then stem from a *convolution* of a particular distribution of diffusivities  $p(K_\alpha)$  for an ensemble of tracers with the Gaussian single-tracer (superstatistical) propagator,

$$P(\delta x, \delta t, K_\alpha) = \exp\left(-\frac{(\delta x)^2}{4K_\alpha(\delta t)^\alpha}\right) / \sqrt{4\pi K_\alpha(\delta t)^\alpha} \quad (21)$$

namely

$$P(x, t) = \int_0^\infty p(K_\alpha) P(\delta x, \delta t, K_\alpha) dK_\alpha, \quad (22)$$

see also Refs.<sup>49,67,107</sup>. Different generalised diffusivities in  $p(K_\alpha)$  can reflect, e.g., large-scale heterogeneities, with the patches of different mucin densities sampled by different tracers. We plan to clarify the limiting behaviour of displacement PDFs for certain realistic  $p(K_\alpha)$  forms<sup>163</sup>. Moreover, we emphasise that the Richardson–Lucy *iterative deconvolution* procedure<sup>160,161</sup> can be employed to the data in order to determine experimentally relevant forms of  $p(K_\alpha)$  from the PDF shapes  $P(x, t)$  measured in experiments<sup>19,20</sup> (see, e.g., the recent study<sup>159</sup>).

*Ageing of mucin hydrogels.* The properties of tracer diffusion in mucin hydrogels crucially depend on the actual sample age<sup>20,30</sup>. This renders control over the starting time of the experiment and the duration of the measurement vitally important for quantifying the dynamics. The effects of a waiting time between the sample preparation and the start of the measurement should be examined in more detail. As shown in Fig. 4.3.11 of Ref.<sup>20</sup>, the effect of ageing of the mucin samples from  $t_a = 1$  to 7 hours at pH=2 leads to a measurable decrease in both the magnitude and the exponent of the TAMSD. In contrast, at pH=7 the effect of sample ageing from  $t_a = 1$  to 8.5 hours is the opposite (and stronger). In Refs.<sup>19,20</sup> the total data-collection time for a sample was about 1 hour, i.e., of the same order as typical ageing time of the mucin gels,  $t_{\text{relax}}$ . As the samples can age during the SPT-measurement<sup>20</sup>, time variation of the model parameters may be important to verify.<sup>194</sup>

*Trajectory length and sample size.* Setting a mini-

mal length for an SPT trajectory,  $N_p^{\min}$ , can bias the final data and outcomes of the analysis. Faster particles quickly leave the focus of the microscope and might not be tracked for a required minimal number of frames, whereas slower particles stay more often in the view-field and, thus, create a bias towards *slower subpopulation* of tracers in the ensemble<sup>17,20,130,164</sup>. In the data sets of Refs.<sup>19,20</sup> the requirement for larger  $N_p^{\min}$  was shown to quickly reduce the number of trajectories. In the current data sets, the traces were limited to 300 points<sup>19</sup>.

Additionally, in particular in non-stationary polymer-based samples with complex internal dynamics, which are also possibly ageing on the timescale of the measurement, collecting a data set with a minimal number of traces,  $N^{\min}$ , can favour slower tracers at later stages of the experiment. This, in turn, creates some *spurious effects* enhancing the weight of slower tracers if larger data sets are collected.<sup>195, 196</sup> Note that the recent developments of approaches based on machine learning and convolutional neural networks for object recognition and automated tracking of particles in two and three dimensions<sup>48</sup>, may provide novel strategies for data acquisition via employing different conditions for minimal trace length, sample size, maximal particle displacements to be recorded, ageing protocols, etc.

*Varying tracer size and surface properties.* Tracer sizes and probe-network interactions were varied in a number of SPT setups with mucin. For instance, PEG-ylated nearly neutral particles at both pH=2 and 7 were studied (the beads were functionalised with a polyethylene-glycol corona), see Ref.<sup>20</sup> also for the original studies on the zeta potential. Analysing additional SPT data with *variable* tracer sizes and surface properties using the current Bayesian approach might help quantifying possible changes in the dominant models of diffusion in these hydrogels under varying experimental conditions.

*Additional statistical quantifiers.* Clearly, a number of other quantifiers can be evaluated for the SPT data sets examined here<sup>19,20</sup>. One more parameter is the so-called asphericity<sup>146,167</sup> that defines the degree of asymmetry<sup>168</sup> of a random walk. Statistical quantifiers involving high-order moments of particle displacements—such as excess kurtosis and the non-Gaussianity parameter<sup>133,149,167</sup>—can also be studied. Fractal dimensions of SPT trajectories<sup>167</sup> and their

space-filling properties can also be quantified, for tracer diffusion in mucin films *in vitro* and in mucus *in vivo*.

*First-passage and target-search properties.* The properties of penetration times of pathogens across mucus layers is also of great applied and theoretical interest, with typical timescales for translocation ranging from tens of minutes to hours<sup>23</sup>. To make some reliable predictions regarding diffusion models describing these translocation events, one would need to perform the Bayesian analysis on much longer time series of tracers in mucus, as compared to 10-sec-long tracks analysed here, Fig. 3. Collecting long traces without intermissions is a great challenge for SPT data-acquisition strategies.

Regarding the search problem, one important feature is the *search efficiency* of mucus-internalised bacteriophage particles for bacterial "prey" cells which are to be infected and destroyed<sup>16</sup>. It would be interesting to investigate this issue in the future, as a function of (tunable) anomalous exponent of phage diffusion, density of phage "predators" and bacterial "prey" cells in the gel, overall mucin concentration, and other relevant parameters.

### Acknowledgments

We thank K. Ribbeck for correspondence and sharing the experimental data of Ref.<sup>19</sup>. A. G. C. thanks I. Goychuk and E. P. Petrov for scientific discussions. C. E. W. was supported by the National Science Foundation (Award DMR-1419807). R. M. acknowledges financial support by the Deutsche Forschungsgemeinschaft (DFG Grants ME 1535/6-1, ME 1535/7-1). R. M. also thanks Foundation for Polish Science within an Alexander von Humboldt Polish Honorary Research Fellowship. S. T. acknowledges the Deutscher Akademischer Austauschdienst for PhD Scholarship (DAAD Program ID 57214224).

**Abbreviations:** single-particle tracking (SPT); mean-squared displacement (MSD); time-averaged mean-squared displacement (TAMSD); probability density function (PDF); diffusing diffusivity (DD); Brownian motion (BM); fractional Brownian motion (FBM); Ornstein-Uhlenbeck (OU).

**Conflict of interests:** There are no conflicts of interest to declare.

\* Electronic address: a.cherstvy@gmail.com

† Electronic address: samudrajit11@gmail.com

‡ Electronic address: cewagner@princeton.edu

§ Electronic address: rmetzler@uni-potsdam.de

<sup>1</sup> M. A. McGuckin, S. K. Linden, P. Sutton, and T. H. Florin, *Mucin dynamics and enteric pathogens*, Nature Rev. Microbiol. **9**, 265 (2011).

<sup>2</sup> B. Button, L.-H. Cai, C. Ehre, M. Kesimer, D. B. Hill, J. K. Sheehan, R. C. Boucher, and M. Rubinstein, *A periciliary brush promotes the lung health by separating the mu-*

*cus layer from airway epithelia*, Science **337**, 937 (2012).

<sup>3</sup> M. G. Roy et al., *Muc5b is required for airway defence*, Nature **505**, 412 (2014).

<sup>4</sup> N. R. Salama, M. L. Hartung, and A. Müller, *Life in the human stomach: persistence strategies of the bacterial pathogen Helicobacter pylori*, Nature Rev. Microbiol. **11**, 385 (2013).

<sup>5</sup> H. Matsui, V. E. Wagner, D. B. Hill, U. E. Schwab, T. D. Rogers, B. Button, R. M. Taylor II, R. Superfine, M. Rubinstein, B. H. Iglewski, and R. C. Boucher, *A physical*

- linkage between cystic fibrosis airway surface dehydration and *Pseudomonas aeruginosa* biofilms, *Proc. Natl. Acad. Sci. U. S. A.* **103**, 18131 (2006).
- <sup>6</sup> B. S. Schuster, J. S. Suk, G. F. Woodworth, and J. Hanes, *Nanoparticle diffusion in respiratory mucus from humans without lung disease*, *Biomaterials* **34**, 3439 (2013).
- <sup>7</sup> J. S. Crater and R. L. Carrier, *Barrier properties of gastrointestinal mucus to nanoparticle transport*, *Macromol. Biosci.* **10**, 1473 (2010).
- <sup>8</sup> S. K. Lai, Y.-Y. Wang, and J. Hanes, *Mucus-penetrating nanoparticles for drug and gene delivery to mucosal tissues*, *Adv. Drug Deliv. Rev.* **61**, 158 (2009).
- <sup>9</sup> O. Lileg, C. Lileg, J. Bloom, C. B. Buck, and K. Ribbeck, *Mucin biopolymers as broad-spectrum antiviral agents*, *Biomacromol.* **13**, 1724 (2012).
- <sup>10</sup> R. A. Cone, *Barrier properties of mucus*, *Adv. Drug Deliv. Rev.* **61**, 75 (2009).
- <sup>11</sup> S. K. Lai, Y.-Y. Wang, K. Hida, R. Cone, and J. Hanes, *Nanoparticles reveal that human cervicovaginal mucus is riddled with pores larger than viruses*, *Proc. Natl. Acad. Sci. U. S. A.* **107**, 598 (2010).
- <sup>12</sup> D. J. Thornton, K. Rousseau, and M. A. McGuckin, *Structure and function of the polymeric mucins in airways mucus*, *Annu. Rev. Physiol.* **70**, 459 (2008).
- <sup>13</sup> O. Lileg, I. Vladescu, and K. Ribbeck, *Characterization of particle translocation through mucin hydrogels*, *Biophys. J.* **98**, 1782 (2010).
- <sup>14</sup> O. Lileg and K. Ribbeck, *Biological hydrogels as selective diffusion barriers*, *Trends Cell Biol.* **21**, 543 (2011).
- <sup>15</sup> L. M. Ensign, B. C. Tang, Y.-Y. Wang, T. A. Tse, T. Hoen, R. Cone, and J. Hanes, *Mucus-penetrating nanoparticles for vaginal drug delivery protect against Herpes Simplex Virus*, *Science Translat. Med.* **4**, 138ra79 (2012).
- <sup>16</sup> J. J. Barr et al., *Subdiffusive motion of bacteriophage in mucosal surfaces increases the frequency of bacterial encounters*, *Proc. Natl. Acad. Sci. U. S. A.* **112**, 13675 (2015).
- <sup>17</sup> J. Witten and K. Ribbeck, *The particle in the spider's web: transport through biological hydrogels*, *Nanoscale* **9**, 8080 (2017).
- <sup>18</sup> J. Witten, T. Samad, and K. Ribbeck, *Selective permeability of mucus barriers*, *Curr. Opin. Biotech.* **52**, 124 (2018).
- <sup>19</sup> C. E. Wagner, B. S. Turner, M. Rubinstein, G. H. McKinley, and K. Ribbeck, *A rheological study of the association and dynamics of MUC5AC gels*, *Biomacromol.* **18**, 3654 (2017).
- <sup>20</sup> C. E. Wagner, PhD Thesis, "Micro- and macro-rheological studies of the structure and association dynamics of biopolymer gels", Massachusetts Institute of Technology, (2018).
- <sup>21</sup> C. E. Wagner et al., *Mucins and their role in shaping the functions of mucus barriers*, *Annu. Rev. Cell Dev. Biol.* **34**, 189 (2018).
- <sup>22</sup> J. J. Barr, R. Auro, M. Furlan, K. L. Whiteson, M. L. Erb, J. Pogliano, A. Stotland, R. Wolkowicz, A. S. Cutting, K. S. Doran, P. Salamon, M. Youle, and F. Rohwer, *Bacteriophage adhering to mucus provide a non-host-derived immunity*, *Proc. Natl. Acad. Sci. U. S. A.* **110**, 10771 (2013).
- <sup>23</sup> M. Lysy, N. S. Pillai, D. B. Hill, M. G. Forest, J. Mellnik, P. Vasquez, and S. A. McKinley, *Model comparison and assessment for single particle tracking in biological fluids*, *J. Amer. Stat.* **111**, 1413 (2016).
- <sup>24</sup> R. G. Schipper, E. Silletti, and M. H. Vingerhoeds, *Saliva as research material: Biochemical, physicochemical and practical aspects*, *Arch. Oral Biol.* **52**, 1114 (2007).
- <sup>25</sup> B. D. E. Raynal, T. E. Hardingham, D. J. Thornton, and J. K. Sheehan, *Concentrated solutions of salivary MUC5B mucin do not replicate the gel-forming properties of saliva*, *Biochem. J.* **362**, 289 (2002).
- <sup>26</sup> E. S. Frenkel and K. Ribbeck, *Salivary mucins in host defense and disease prevention*, *J. Oral Microbiol.* **7**, 29759 (2015).
- <sup>27</sup> D. B. Hill et al., *A biophysical basis for mucus solids concentration as a candidate biomarker for airways disease*, *PLoS ONE* **9**, e87681 (2014).
- <sup>28</sup> J. P. Celli, B. S. Turner, N. H. Afdhal, S. Keates, I. Ghirani, C. P. Kelly, R. H. Ewoldt, G. H. McKinley, P. So, S. Erramilli, and R. Bansil, *Helicobacter pylori moves through mucus by reducing mucin viscoelasticity*, *Proc. Natl. Acad. Sci. U. S. A.* **106**, 14321 (2009).
- <sup>29</sup> M. E. V. Johansson, H. Sjövall, and G. C. Hansson, *The gastrointestinal mucus system in health and disease*, *Nature Rev. Gastroent. & Hepat.* **10**, 352 (2013).
- <sup>30</sup> A.-M. Philippe, L. Cipelletti, and D. Larobina, *Mucus as an arrested phase separation gel*, *Macromol.* **50**, 8221 (2017).
- <sup>31</sup> C. Su, M. Padra, M. A. Constantino, S. Sharba, A. Thorell, S. K. Linden, and R. Bansil, *Influence of the viscosity of healthy and diseased human mucins on the motility of Helicobacter pylori*, *Sci. Rep.* **8**, 9710 (2018).
- <sup>32</sup> K. B. Smith-Dupont, C. E. Wagner, J. Witten, K. Conroy, H. Rudoltz, K. Pagidas, V. Snegovskikh, M. House, and K. Ribbeck, *Probing the potential of mucus permeability to signify preterm birth risk*, *Sci. Rep.* **7**, 10302 (2017).
- <sup>33</sup> H. Corvol et al., *Genome-wide association meta-analysis identifies five modifier loci of lung disease severity in cystic fibrosis*, *Nature Comm.* **6**, 8382 (2015).
- <sup>34</sup> A. W. Larhed, P. Artursson, J. Grasjo, and E. Björk, *Diffusion of drugs in native and purified gastrointestinal mucus*, *J. Pharm. Sci.* **86**, 660 (1997).
- <sup>35</sup> A.-C. Groo and F. Lagarce, *Mucus models to evaluate nanomedicines for diffusion*, *Drug Disc. Today* **19**, 1097 (2014).
- <sup>36</sup> K. H. Bae, L.-S. Wang, and M. Kurisawa, *Injectable biodegradable hydrogels: progress and challenges*, *J. Mater. Chem. B* **1**, 5371 (2013).
- <sup>37</sup> T. A. Waigh, *Microrheology of complex fluids*, *Rep. Prog. Phys.* **68**, 685 (2005).
- <sup>38</sup> D. Wirtz, *Particle-tracking microrheology of living cells: Principles and applications*, *Annu. Rev. Biophys.* **38**, 301 (2009).
- <sup>39</sup> J. Hansing, J. R. Duke, E. B. Fryman, J. E. DeRouchey, and R. R. Netz, *Particle diffusion in polymeric hydrogels with mixed attractive and repulsive interactions*, *Nano Lett.* **18**, 5248 (2018).
- <sup>40</sup> J. Hansing and R. R. Netz, *Hydrodynamic effects on particle diffusion in polymeric hydrogels with steric and electrostatic particle-gel interactions*, *Macromol.* **51**, 7608 (2018).
- <sup>41</sup> C. P. Goodrich, M. P. Brenner, and K. Ribbeck, *Enhanced diffusion by binding to the crosslinks of a polymer gel*, *Nature Comm.* **9**, 4348 (2018).
- <sup>42</sup> S. K. Ghosh, A. G. Cherstvy, and R. Metzler, *Non-universal tracer diffusion in crowded media of non-inert obstacles*, *Phys. Chem. Chem. Phys.* **17**, 1847 (2015).

- <sup>43</sup> J. Shin, A. G. Cherstvy, and R. Metzler, *Sensing viruses by mechanical tension of DNA in responsive hydrogels*, Phys. Rev. X **4**, 021002 (2014).
- <sup>44</sup> M. T. Valentine, P. D. Kaplan, D. Thota, J. C. Crocker, T. Gisler, R. K. Prud'homme, M. Beck, and D. A. Weitz, *Investigating the microenvironments of inhomogeneous soft materials with multiple particle tracking*, Phys. Rev. E **64**, 061506 (2001).
- <sup>45</sup> I. Y. Wong, M. L. Gardel, D. R. Reichman, E. R. Weeks, M. T. Valentine, A. R. Bausch, and D. A. Weitz, *Anomalous diffusion probes microstructure dynamics of entangled F-actin networks*, Phys. Rev. Lett. **92**, 178101 (2004).
- <sup>46</sup> N. Gal, D. Lechtman-Goldstein, and D. Weihs, *Particle tracking in living cells: a review of the mean square displacement method and beyond*, Rheol. Acta **52**, 425 (2013).
- <sup>47</sup> C. Manzo and M. F. Garcia-Parajo, *A review of progress in single particle tracking: from methods to biophysical insights*, Rep. Prog. Phys. **78**, 124601 (2015).
- <sup>48</sup> J. M. Newby, A. M. Schaefer, P. T. Lee, M. G. Forest, and S. K. Lai, *Convolutional neural networks automate detection for tracking of submicron-scale particles in 2D and 3D*, Proc. Natl. Acad. Sci. U. S. A. **115**, 9026 (2018).
- <sup>49</sup> S. Thapa, J. Krog, M. A. Lomholt, A. G. Cherstvy, and R. Metzler, *Bayesian analysis of single-particle tracking data using the nested-sampling algorithm: maximum-likelihood model selection applied to stochastic-diffusivity data*, Phys. Chem. Chem. Phys. **20**, 29018 (2018).
- <sup>50</sup> H. Jeffreys, "Theory of Probability", (Clarendon Press, Oxford, 1939); H. Jeffreys, "Scientific Inference", (Cambridge University Press, Cambridge, 1957).
- <sup>51</sup> C. J. D. MacKay, "Information Theory, Inference and Learning Algorithms", (Cambridge University Press, 2003).
- <sup>52</sup> S. D. Sivia and J. Skilling, "Data Analysis: A Bayesian Tutorial", (Oxford University Press, 2006).
- <sup>53</sup> T. E. Jaynes and L. G. Bretthorst, "Probability Theory—The Logic of Science", (Cambridge University Press, 2003).
- <sup>54</sup> J. Skilling, *Nested sampling*, AIP Conf. Proc. **735**, 395 (2004).
- <sup>55</sup> J. Skilling, *Nested sampling for general Bayesian computation*, Bayesian Anal. **1**, 833 (2006).
- <sup>56</sup> J. Skilling, "Nested sampling for Bayesian computations", Proc. Valencia, ISBA 8th World meeting on Bayesian Statistics, Benidorm (Alicante, Spain), June 1st-6th, (2006).
- <sup>57</sup> R. Trotta, *Bayes in the sky: Bayesian inference and model selection in cosmology*, Contemp. Physics **49**, 71 (2008).
- <sup>58</sup> R. Trotta, G. Jóhannesson, I. V. Moskalenko, T. A. Porter, R. Ruiz de Austri, and A. W. Strong, *Constraints in cosmic-ray propagation models from global Bayesian analysis*, Astrophys. J. **729**, 106 (2011).
- <sup>59</sup> H. Jeffreys, *An invariant form for the prior probability in estimation problems*, Proc. R. Soc. Lond. A **186**, 453 (1946).
- <sup>60</sup> P. Langevin, *Sur la théorie de mouvement brownien*, C. R. Hebd. Seances Acad. Sci. **146**, 530 (1908).
- <sup>61</sup> J. Krog and M. A. Lomholt, *Bayesian inference with information content model check for Langevin equations*, Phys. Rev. E **96**, 062106 (2017).
- <sup>62</sup> V. Dose, *Bayesian inference in physics: case studies*, Rep. Prog. Phys. **66**, 1421 (2003).
- <sup>63</sup> J. Krog, L. H. Jacobsen, F. W. Lund, D. Wüstner, and M. A. Lomholt, *Bayesian model selection with fractional Brownian motion*, arXiv:1804.01365.
- <sup>64</sup> B. B. Mandelbrot and W. J. van Ness, *Fractional Brownian motions, fractional noises and applications*, SIAM Rev. **10**, 422 (1968).
- <sup>65</sup> B. B. Mandelbrot, "The Fractal Geometry of Nature", (W. H. Freeman, New York, 1982).
- <sup>66</sup> R. Metzler, J.-H. Jeon, A. G. Cherstvy, and E. Barkai, *Anomalous diffusion models and their properties: non-stationarity, non-ergodicity, and ageing at the centenary of single particle tracking*, Phys. Chem. Chem. Phys. **16**, 24128 (2014).
- <sup>67</sup> A. V. Chechkin, F. Seno, R. Metzler, and I. M. Sokolov, *Brownian yet non-Gaussian diffusion: from superstatistics to subordination of diffusing diffusivities*, Phys. Rev. X **7**, 021002 (2017).
- <sup>68</sup> G. E. Uhlenbeck and L. S. Ornstein, *On the theory of the Brownian motion*, Phys. Rev. **36**, 823 (1930).
- <sup>69</sup> S. Chandrasekhar, *Stochastic problems in physics and astronomy*, Rev. Mod. Phys. **15**, 1 (1943).
- <sup>70</sup> J.-P. Bouchaud and A. Georges, *Anomalous diffusion in disordered media: Statistical mechanisms, models and physical applications*, Phys. Rep. **195**, 127 (1990).
- <sup>71</sup> R. Metzler and J. Klafter, *The random walk's guide to anomalous diffusion: a fractional dynamics approach*, Phys. Rep. **339**, 1 (2000).
- <sup>72</sup> R. Metzler and J. Klafter, *The restaurant at the end of the random walk: recent developments in the description of anomalous transport by fractional dynamics*, J. Phys. A **37**, R161 (2004).
- <sup>73</sup> Y. He, S. Burov, R. Metzler, and E. Barkai, *Random time-scale invariant diffusion and transport coefficients*, Phys. Rev. Lett. **101**, 058101 (2008).
- <sup>74</sup> S. Burov, J.-H. Jeon, R. Metzler, and E. Barkai, *Single particle tracking in systems showing anomalous diffusion: the role of weak ergodicity breaking*, Phys. Chem. Chem. Phys. **13**, 1800 (2011).
- <sup>75</sup> J.-H. Jeon, V. Tejedor, S. Burov, E. Barkai, C. Selhuber-Unkel, K. Berg-Sørensen, L. Oddershede, and R. Metzler, *In vivo anomalous diffusion and weak ergodicity breaking of lipid granules*, Phys. Rev. Lett. **106**, 048103 (2011).
- <sup>76</sup> I. M. Sokolov, *Models of anomalous diffusion in crowded environments*, Soft Matter **8**, 9043 (2012).
- <sup>77</sup> F. Höfling and T. Franosch, *Anomalous transport in the crowded world of biological cells*, Rep. Prog. Phys. **76**, 046602 (2013).
- <sup>78</sup> Y. Meroz and I. M. Sokolov, *A toolbox for determining subdiffusive mechanisms*, Phys. Rep. **573**, 1 (2015).
- <sup>79</sup> R. Metzler, J.-H. Jeon, and A. G. Cherstvy, *Non-Brownian diffusion in lipid membranes: experiments and simulations*, Biochim. Biophys. Acta BBA-Biomembr. **1858**, 2451 (2016).
- <sup>80</sup> K. Nørregaard, R. Metzler, C. Ritter, K. Berg-Sørensen, and L. Oddershede, *Manipulation and motion of organelles and single molecules in living cells*, Chem. Rev. **117**, 4342 (2017).
- <sup>81</sup> A. G. Cherstvy and R. Metzler, *Nonergodicity, fluctuations, and criticality in heterogeneous diffusion processes*, Phys. Rev. E **90**, 012134 (2014).
- <sup>82</sup> A. G. Cherstvy, and R. Metzler, *Anomalous diffusion in time-fluctuating non-stationary diffusivity landscapes*, Phys. Chem. Chem. Phys. **18**, 23840 (2016).
- <sup>83</sup> F. Le Vot, E. Abad, and S. B. Yuste, *Continuous-time random-walk model for anomalous diffusion in expanding*

- media*, Phys. Rev. E **96**, 032117 (2017).
- <sup>84</sup> J. L. Lebowitz and O. Penrose, *Modern ergodic theory*, Phys. Today **26**, 23 (1973).
- <sup>85</sup> C. C. Moore, *Ergodic theorem, ergodic theory, and statistical mechanics*, Proc. Natl. Acad. Sci. U. S. A. **112**, 1907 (2015).
- <sup>86</sup> W. Deng and E. Barkai, *Ergodic properties of fractional Brownian-Langevin motion*, Phys. Rev. E **79**, 011112 (2009).
- <sup>87</sup> S. Hapca, J. W. Crawford, and I. M. Young, *Anomalous diffusion of heterogeneous populations characterized by normal diffusion at the individual level*, J. Roy. Soc. Interface **6**, 111 (2009).
- <sup>88</sup> B. Wang, S. M. Anthony, S. C. Bae, and S. Granick, *Anomalous yet Brownian*, Proc. Natl. Acad. Sci. U. S. A. **106**, 15160 (2009).
- <sup>89</sup> B. Wang, J. Kuo, S. C. Bae, and S. Granick, *When Brownian diffusion is not Gaussian*, Nature Mater. **11**, 481 (2012).
- <sup>90</sup> A. Rahman, *Correlations in the motion of atoms in liquid argon*, Phys. Rev. **136**, A405 (1964).
- <sup>91</sup> S. K. Ghosh, A. G. Cherstvy, D. S. Grebenkov, and R. Metzler, *Anomalous, non-Gaussian tracer diffusion in crowded two-dimensional environments*, New J. Phys. **18**, 013027 (2016).
- <sup>92</sup> L.-H. Cai, S. Panyukov, and M. Rubinstein, *Mobility of nonsticky nanoparticles in polymer liquids*, Macromol. **44**, 7853 (2011).
- <sup>93</sup> J. T. Kalathi, U. Yamamoto, K. S. Schweizer, G. S. Grest, and S. K. Kumar, *Nanoparticle diffusion in polymer nanocomposites*, Phys. Rev. Lett. **112**, 108301 (2014).
- <sup>94</sup> L.-H. Cai, S. Panyukov, and M. Rubinstein, *Hopping diffusion of nanoparticles in polymer matrices*, Macromol. **48**, 847 (2015).
- <sup>95</sup> T. Toyota, D. A. Head, C. F. Schmidt, and D. Mizuno, *Non-Gaussian athermal fluctuations in active gels*, Soft Matter **7**, 3234 (2011).
- <sup>96</sup> U. Yamamoto and K. S. Schweizer, *Theory of nanoparticle diffusion in unentangled and entangled polymer melts*, J. Chem. Phys. **135**, 224902 (2011).
- <sup>97</sup> P. Polanowski and A. Sikorski, *Diffusion of small particles in polymer films*, J. Chem. Phys. **147**, 014902 (2017).
- <sup>98</sup> M. S. Song, H. C. Moon, J.-H. Jeon, H. Y. Park, *Neuronal messenger ribonucleoprotein transport follows an aging Lévy walk*, Nature Comm. **9**, 344 (2018).
- <sup>99</sup> R. Keidel, A. Ghavami, D. M. Lugo, G. Lotze, O. Virtanen, P. Beumers, J. S. Pedersen, A. Bardow, R. G. Winkler, and W. Richtering, *Time-resolved structural evolution during the collapse of responsive hydrogels: The microgel-to-particle transition*, Sci. Adv. **4**, eaao7086 (2018).
- <sup>100</sup> M. V. Chubynsky and G. W. Slater, *Diffusing diffusivity: a model for anomalous, yet Brownian, diffusion*, Phys. Rev. Lett. **113**, 098302 (2014).
- <sup>101</sup> R. Jain and K. L. Sebastian, *Diffusion in a crowded, rearranging environment*, J. Phys. Chem. B **120**, 3988 (2016).
- <sup>102</sup> R. Jain and K. L. Sebastian, *Lévy flight with absorption: a model for diffusing diffusivity with long tails*, Phys. Rev. E **95**, 032135 (2017).
- <sup>103</sup> E. Yamamoto, T. Akimoto, A. C. Kalli, K. Yasuoka, and M. S. P. Sansom, *Dynamic interactions between a membrane binding protein and lipids induce fluctuating diffusivity*, Science Adv. **3**, e1601871 (2017).
- <sup>104</sup> J. Guan, B. Wang, and S. Granick, *Even hard-sphere colloidal suspensions display Fickian yet non-Gaussian diffusion*, ACS Nano **8**, 3331 (2014).
- <sup>105</sup> D. Wang, C. He, M. P. Stoykovich, and D. K. Schwartz, *Nanoscale topography influences polymer surface diffusion*, ACS Nano **9**, 1656 (2015).
- <sup>106</sup> T. J. Lampo, S. Stylianidou, M. P. Backlund, P. A. Wiggins, and A. J. Spakowitz, *Cytoplasmic RNA-protein particles exhibit non-Gaussian subdiffusive behavior*, Biophys. J. **112**, 1 (2017).
- <sup>107</sup> A. G. Cherstvy, O. Nagel, C. Beta, and R. Metzler, *Non-Gaussianity, population heterogeneity, and transient superdiffusion in the spreading dynamics of amoeboid cells*, Phys. Chem. Chem. Phys. **20**, 23034 (2018).
- <sup>108</sup> J. Slezak, R. Metzler, and M. Magdziarz, *Superstatistical generalised Langevin equation: non-Gaussian viscoelastic anomalous diffusion*, New J. Phys. **20**, 023026 (2018).
- <sup>109</sup> V. Sposini, A. V. Chechkin, F. Seno, G. Pagnini, and R. Metzler, *Random diffusivity from stochastic equations: comparison of two models for Brownian yet non-Gaussian diffusion*, New J. Phys. **20**, 043044 (2018).
- <sup>110</sup> C. Metzner, C. Mark, J. Steinwachs, L. Lautscham, F. Stadler, and B. Fabry, *Superstatistical analysis and modelling of heterogeneous random walks*, Nature Comm. **6**, 7516 (2015).
- <sup>111</sup> M. J. Skaug and D. K. Schwartz, *Tracking nanoparticle diffusion in porous filtration media*, Ind. Eng. Chem. Res. **54**, 4414 (2015).
- <sup>112</sup> S. Sadegh, J. L. Higgins, P. C. Mannion, M. M. Tamkun, and D. Krapf, *Plasma membrane is compartmentalized by a self-similar cortical actin meshwork*, Phys. Rev. X **7**, 011031 (2017).
- <sup>113</sup> R. Motohashi and I. Hanasaki, *Characterization of aqueous cellulose nanofiber dispersions from microscopy movie data of Brownian particles by trajectory analysis*, Nanoscale Adv. **1**, 421 (2019).
- <sup>114</sup> A. G. Cherstvy, S. Thapa, Y. Mardoukhi, A. V. Chechkin, and R. Metzler, *Time averaged and ergodic properties of the Ornstein-Uhlenbeck process: particle starting distributions and relaxation to stationarity*, Phys. Rev. E **98**, 022134 (2018).
- <sup>115</sup> E. R. Weeks and D. A. Weitz, *Subdiffusion and the cage effect studied near the colloidal glass transition*, Chem. Phys. **284**, 361 (2002).
- <sup>116</sup> E. R. Weeks and D. A. Weitz, *Properties of cage rearrangements observed near the colloidal glass transition*, Phys. Rev. Lett. **89**, 095704 (2002).
- <sup>117</sup> C. Beck and E. G. D. Cohen, *Superstatistics*, Physica A **322**, 267 (2003).
- <sup>118</sup> C. Beck, *Superstatistical Brownian motion*, Prog. Theor. Phys. Suppl. **162**, 29 (2006).
- <sup>119</sup> T. Bayes, *An essay toward solving a problem in the doctrine of chances*, Phil. Trans. Roy. Soc. **63**, 370 (1763).
- <sup>120</sup> P. C. Gregory, "Bayesian Logical Data Analysis for the Physical Sciences", (Cambridge University Press, Cambridge, 2005).
- <sup>121</sup> G. D'Agostini, *Bayesian inference in processing experimental data: principles and basic applications*, Rep. Prog. Phys. **66**, 1383 (2003).
- <sup>122</sup> U. von Toussaint, *Bayesian inference in physics*, Rev. Mod. Phys. **83**, 943 (2011).
- <sup>123</sup> N. Monnier, S. M. Guo, M. Mori, J. He, P. Lenart, and M. Bathe, *Bayesian approach to MSD-based analysis of particle motion in live cells*, Biophys. J. **103**, 616 (2012).
- <sup>124</sup> A. N. Kolmogorov, *Wienersche Spiralen und einige an-*

- dere interessante Kurven im Hilbertschen Raum*, C. R. (Doklady) Acad. Sci. U. R. S. S. (N. S.) **26**, 115 (1940).
- <sup>125</sup> FBM-code: <https://github.com/mlomholt/fbm>; DD-code: [https://github.com/samudrajit11/ns\\_dd](https://github.com/samudrajit11/ns_dd).
- <sup>126</sup> A. G. Cherstvy, *Effect of a low-dielectric interior on DNA electrostatic response to twisting and bending*, J. Phys. Chem. B **111**, 12933 (2007).
- <sup>127</sup> A. G. Cherstvy and V. B. Teif, *Electrostatic effect of H1-histone protein binding on nucleosome repeat length*, Phys. Biol. **11**, 044001 (2014).
- <sup>128</sup> We refer here to <http://tacaswell.github.io/tracking/html/>, <http://www.physics.emory.edu/faculty/weeks/idl/>, <http://physics.nyu.edu/grierlab/software.html>, and <http://site.physics.georgetown.edu/matlab/>.
- <sup>129</sup> T. Savin and P. S. Doyle, *Static and dynamic errors in particle tracking microrheology*, Biophys. J. **88**, 623 (2005).
- <sup>130</sup> F. Etoc, E. Balloul, C. Vicario, D. Normanno, D. Liße, A. Sittner, J. Piehler, M. Dahan, and M. Coppey, *Non-specific interactions govern cytosolic diffusion of nano-sized objects in mammalian cells*, Nature Mater. **17**, 740 (2018).
- <sup>131</sup> A. A. Sadoon and Y. Wang, *Anomalous, non-Gaussian, viscoelastic, and age-dependent dynamics of histonelike nucleoid-structuring proteins in live Escherichia coli*, Phys. Rev. E **98**, 042411 (2018).
- <sup>132</sup> J.-H. Jeon, M. Javanainen, H. Martinez-Seara, R. Metzler, and I. Vattulainen, *Protein crowding in lipid bilayers gives rise to non-Gaussian anomalous lateral diffusion of phospholipids and proteins*, Phys. Rev. X **6**, 021006 (2016).
- <sup>133</sup> J. Mellnik, P. A. Vasquez, S. A. McKinley, J. Witten, D. B. Hill, and M. G. Forest, *Micro-heterogeneity metrics for diffusion in soft matter*, Soft Matter **10**, 7781 (2014).
- <sup>134</sup> J.-H. Jeon, N. Leijnse, L. B. Oddershede, and R. Metzler, *Anomalous diffusion and power-law relaxation of the time averaged mean squared displacement in worm-like micellar solutions*, New J. Phys. **15**, 045011 (2013).
- <sup>135</sup> Y. Matsuda, I. Hanasaki, R. Iwao, H. Yamaguchi, and T. Niimi, *Estimation of diffusive states from single-particle trajectory in heterogeneous medium using machine-learning methods*, Phys. Chem. Chem. Phys. **20**, 24099 (2018).
- <sup>136</sup> D. Montiel, H. Cang, and H. Yang, *Quantitative characterization of changes in dynamical behavior for single-particle tracking studies*, J. Phys. Chem. B **110**, 19763 (2006).
- <sup>137</sup> D. S. Martin, M. B. Forstner, and J. A. Käs, *Apparent subdiffusion inherent to single particle tracking*, Biophys. J. **83**, 2109 (2002).
- <sup>138</sup> X. Michalet, *Mean square displacement analysis of single-particle trajectories with localization error: Brownian motion in an isotropic medium*, Phys. Rev. E **82**, 041914 (2010).
- <sup>139</sup> X. Michalet and A. J. Berglund, *Optimal diffusion coefficient estimation in single-particle tracking*, Phys. Rev. E **85**, 061916 (2012).
- <sup>140</sup> K. Burnecki, E. Kepten, Y. Garini, G. Sikora, and A. Weron, *Estimating the anomalous diffusion exponent for single particle tracking data with measurement errors - An alternative approach*, Sci. Rep. **5**, 11306 (2015).
- <sup>141</sup> C. L. Vestergaard, P. C. Blainey, and H. Flyvbjerg, *Optimal estimation of diffusion coefficients from single-particle trajectories*, Phys. Rev. E **89**, 022726 (2014).
- <sup>142</sup> K. Burnecki, E. Kepten, J. Janczura, I. Bronshtein, Y. Garini, and A. Weron, *Universal algorithm for identification of fractional Brownian motion. A case of telomere subdiffusion*, Biophys. J. **103**, 1839 (2012).
- <sup>143</sup> D. C. Young and J. Scrimgeour, *Optimizing likelihood models for particle trajectory segmentation in multi-state systems*, Phys. Biol. **15**, 066003 (2018).
- <sup>144</sup> S. K. Lai, Y.-Y. Wang, D. Wirtz and J. Hanes, *Micro- and macrorheology of mucus*, Adv. Drug Deliv. Rev. **61**, 86 (2009).
- <sup>145</sup> S. K. Lai, D. E. O'Hanlon, S. Harrold, S. T. Man, Y.-Y. Wang, R. Cone, and J. Hanes, *Rapid transport of large polymeric nanoparticles in fresh undiluted human mucus*, Proc. Natl. Acad. Sci. U. S. A. **104**, 1482 (2007).
- <sup>146</sup> K. Speckner, L. Stadler, and M. Weiss, *Anomalous dynamics of the endoplasmic reticulum network*, Phys. Rev. E **98**, 012406 (2018).
- <sup>147</sup> A. G. Cherstvy and R. Metzler, *Population splitting, trapping, and non-ergodicity in heterogeneous diffusion processes*, Phys. Chem. Chem. Phys. **15**, 20220 (2013).
- <sup>148</sup> A. Andrianov and D. S. Grebenkov, *Time-averaged MSD of Brownian Motion*, J. Stat. Mech. **P07001**, (2012).
- <sup>149</sup> M. Schwarzl, A. Godec, and R. Metzler, *Quantifying non-ergodicity of anomalous diffusion with higher order moments*, Sci. Rep. **7**, 3878 (2017).
- <sup>150</sup> R. Hou, A. G. Cherstvy, R. Metzler, and T. Akimoto, *Biased continuous-time random walks for ordinary and equilibrium cases: facilitation of diffusion, ergodicity breaking and ageing*, Phys. Chem. Chem. Phys. **20**, 20827 (2018).
- <sup>151</sup> A. G. Cherstvy, A. V. Chechkin and R. Metzler, *Anomalous diffusion and ergodicity breaking in heterogeneous diffusion processes*, New J. Phys. **15**, 083039 (2013).
- <sup>152</sup> A. G. Cherstvy and R. Metzler, *Ergodicity breaking, ageing, and confinement in generalized diffusion processes with position and time dependent diffusivity*, J. Stat. Mech. **P05010**, (2015).
- <sup>153</sup> H. Safdari, A. G. Cherstvy, A. V. Chechkin, F. Thiel, I. M. Sokolov, and R. Metzler, *Quantifying the non-ergodicity of scaled Brownian motion*, J. Phys. A **48**, 375002 (2015).
- <sup>154</sup> A. V. Weigel, B. Simon, M. M. Tamkun, and D. Krapf, *Ergodic and nonergodic processes coexist in the plasma membrane as observed by single-molecule tracking*, Proc. Natl. Acad. Sci. U. S. A. **108**, 6438 (2011).
- <sup>155</sup> J. H. P. Schulz, E. Barkai, and R. Metzler, *Ageing effects and population splitting in single-particle trajectory averages*, Phys. Rev. Lett. **110**, 020602 (2013).
- <sup>156</sup> J. H. P. Schulz, E. Barkai, and R. Metzler, *Ageing renewal theory and application to random walks*, Phys. Rev. X **4**, 011028 (2014).
- <sup>157</sup> H. Loch-Olszewska and J. Szwabiński, *Detection of  $\epsilon$ -ergodicity breaking in experimental data—A study of the dynamical functional sensibility*, J. Chem. Phys. **148**, 204105 (2018).
- <sup>158</sup> J. F. Reverey, J.-H. Jeon, H. Bao, M. Leippe, R. Metzler, and C. Selhuber-Unkel, *Superdiffusion dominates intracellular particle motion in the supercrowded cytoplasm of pathogenic Acanthamoeba castellanii*, Sci. Rep. **5**, 11690 (2015).
- <sup>159</sup> W. Hong, G. Xu, X. Ou, W. Sun, T. Wang, and Z. Tong, *Colloidal probe dynamics in gelatin solution during the solgel transition*, Soft Matter **14**, 3694 (2018).
- <sup>160</sup> W. H. Richardson, *Bayesian-based iterative method of image restoration*, J. Opt. Soc. Amer. **62**, 55 (1972).
- <sup>161</sup> L. B. Lucy, *An iterative technique for the rectification of*

- observed distributions, *Astron. J.* **79**, 745 (1974).
- 162 J. W. R. Mellnik et al., *Maximum likelihood estimation for single particle, passive microrheology data with drift*, *J. Rheol.* **60**, 379 (2016).
- 163 A. G. Cherstvy et al., work in progress, (2018).
- 164 Y. Golan and E. Sherman, *Resolving mixed mechanisms of protein subdiffusion at the T cell plasma membrane*, *Nature Comm.* **8**, 15851 (2017).
- 165 C. Mark, C. Metzner, L. Lautscham, P. L. Strissel, R. Strick, and B. Fabry, *Bayesian model selection for complex dynamic systems*, *Nature Comm.* **9**, 1803 (2018).
- 166 S. L. Heston, *A closed-form solution for options with stochastic volatility with applications to bond and currency options*, *Rev. Financ. Stud.* **6**, 327 (1993).
- 167 T. Wagner, A. Kroll, C. R. Haramagatti, H.-G. Lipinski, and M. Wiemann, *Classification and segmentation of nanoparticle diffusion trajectories in cellular micro environments*, *PLoS ONE* **12**, e0170165 (2017).
- 168 J. Rudnick and G. Gaspari, *The shapes of random walks*, *Science* **237**, 384 (1987).
- 169 *Helicobacter pylori* is believed to increase its motility in gastric mucus by hydrolyzing urea, thus raising the pH level of the surrounding gel and reducing its viscoelasticity<sup>13,31</sup>. During the ovulatory phase of the female menstrual cycle, cervical mucus is up to  $\sim 10^2$  times<sup>8</sup> less viscoelastic at low shear<sup>10</sup>, facilitating the passage of sperm cells. Cervical mucus forms a protective barrier at natural pH, while during ovulation the pH is reduced, enabling sperm penetration (but also reducing protection against certain pathogens<sup>13</sup>). The permeability of cervicovaginal mucus to micron-sized tracers was also studied to quantify the risk of pre-term birth<sup>32</sup>. Some methods for preventing sexually transmitted infections—including vaginal human immunodeficiency virus—involve manipulations of vaginal mucus<sup>15</sup>.
- 170 The viscosity of native mucus is similar to that of mayonnaise<sup>10</sup>: at low shear rates mucus is  $\gtrsim 10^3$  more viscous than water<sup>8</sup>. For passive microrheology, the underlying "microenvironments"<sup>44–46</sup> of mucin films predispose the properties of thermally agitated transport of (sub)micron-sized particles. For mucin gels, mechanical stability, elastic moduli, degree of cross-linking, network heterogeneity, and its permeability all sensitively depend on the pH level and the amount of added salt(s)<sup>20</sup>. Note that the apparent gel viscosity for  $0.1\text{-}\mu\text{m}$  tracers at  $\delta t = 1$  sec can be  $16\times$  larger than that for  $1\text{-}\mu\text{m}$  probes<sup>20</sup>.
- 171 Although some properties of tracer diffusion in native mucus can be mimicked by proper conditions in gels reconstituted from purified mucins<sup>27</sup>, some *major discrepancies* were detected, see, e.g., Ref.<sup>25</sup> for the example of saliva.
- 172 It was shown<sup>30</sup>, e.g., that both non-aged and aged mucin samples of pig gastric mucus reveal similar morphologies of interconnected  $\sim 5\text{--}10\text{ }\mu\text{m}$ -large *pores* in the network. Static light-scattering measurements have also shown that non-aged samples are quite homogeneous on large scales (small- $q$  regime). For the aged samples, the scattering intensity for small  $q$  values  $q \sim 0.1\text{--}1\text{ }\mu\text{m}^{-1}$  increases, indicative of large-scale density fluctuations and the onset on phase separation<sup>30</sup>. For aged samples the typical timescale is  $t_{\text{relax}} \sim 10\text{--}100\text{ min}$ <sup>30</sup>. Some rearrangements of the gel's microscopic structure with age include a growth of dense domains in the network and subsequent "merging" events<sup>30</sup>. The network connectivity then decreases and its elastic modulus is reduced<sup>20,30</sup>.
- The network dynamics<sup>1,6</sup> slows down as the mucin sample ages and correlation distances increase vastly with sample age, reaching  $\sim\text{mm}$  scale<sup>30</sup> (as in the "gelation" effect).
- 173 The importance of different microenvironments for tracer diffusion in inhomogeneous media was emphasised previously<sup>44</sup>. This study presents the (first) quantitative analysis of non-Gaussian, nearly exponential PDFs for diffusion of micron-sized tracers in heterogeneous media, such as agarose gels. The authors observed the presence of varying local microenvironments and particle-to-particle variations in diffusivities<sup>44</sup>, laying the foundation for the DD-based models<sup>67,87,100</sup>. The effect of non-Gaussianity and cage rearrangement were also emphasised<sup>115,116</sup>, with for cooperative motion of neighbouring particles and longer-than-Gaussian tails emerging for self-diffusion in dense colloidal suspensions due to long-range jumps into newly opened cages.
- 174 The effect of added salt on elasticity and stability of mucin networks is two-fold. From the point of view of persistence of a polyampholyte-like mucin chain, its rigidity at higher salt amounts should decrease due to better Debye-Hückel screening of charges<sup>19</sup>, see also Refs.<sup>126,127</sup>. Also, at higher salt amounts the intermolecular repulsions between mucin chains are weakened, so the (salt-insensitive) crosslinks between the chains may live longer (dissociate less frequently)<sup>19</sup>. The viscoelastic moduli of mucin gels grow substantially as salt concentration increases from 0 to 400 mM at pH=7, see Fig. 2b of Ref.<sup>19</sup>. Upon this change in salinity, tracer motion becomes progressively subdiffusive, but the Gaussian PDF is still preserved<sup>19</sup>. We refer to Ref.<sup>20</sup> for the discussion of effects of added salt on the charge density of mucin chains and tracer beads.
- 175 With increasing  $n_0$  at pH=7 the magnitude of  $\overline{\delta_i^2(\Delta)}$  and their exponent  $\beta_i$  decrease substantially, Fig. 4b in Ref.<sup>19</sup> (not shown). This trend of decreasing particle mobility (more confined motion) is corroborated by an increasing elastic modulus of the network at higher salt concentrations,  $n_0$ . Overall, however, the maximal tracer displacements often remain very small,  $\overline{\delta^2(\Delta_{\text{max}})} \sim 0.1\text{--}1\text{ }\mu\text{m}$ . This "jiggling"-like tracer motion occurs on scales *smaller* than its own diameter (similar to Ref.<sup>75</sup>).
- 176 SPT experiments<sup>19</sup> sometimes faced technical difficulties with *dedrifting* fast and slow particles in the same image for strongly heterogeneous gels. This could potentially give rise to *superdiffusive behaviours* for the fastest particles (Crocker-Grier-Weeks-Kilfoil dedrifting scheme<sup>128</sup> was employed in Refs.<sup>19,20</sup>). We mention here, however, the recently proposed physical mechanism of facilitation of tracer diffusion via binding to hydrogel and disrupting its polymer crosslinks<sup>41</sup>. We also refer to the discussion of superdiffusive exponents in Ref.<sup>131</sup>.
- 177 A similar separation of subdiffusive tracers was performed for F-actin networks in Ref.<sup>45</sup>. The population was split into predominantly diffusive particles and tracers strongly confined to local microenvironments and only rarely hopping between "cages" of the network. These hops result in progressively *subdiffusive* MSDs for particle spreading in entangled F-actin networks at increasing polymer concentrations<sup>45</sup>. In theory, the events of *particle hopping* can also be realisable for "slow" tracers confined in "cages" of mucin hydrogels<sup>19,20</sup>, but likely on timescales much longer than those probed originally<sup>19</sup>.
- 178 These results can be compared to findings of Ref.<sup>132</sup>

in which protein crowding on lipid bilayers was demonstrated by computer simulations to give rise to intermittently confined particles, broad distributions of diffusion coefficients,  $p(D)$ , and non-Gaussian PDFs of particle displacements.

<sup>179</sup> At pH=7—despite increasing viscoelastic moduli of the gel with addition of salt (from  $n_0 = 0$  to 0.4 M)<sup>20</sup>—the mucin network stays quite homogeneous, with fairly Gaussian PDFs and small HR values<sup>19</sup>. Note that a decomposition of tracer trajectories into *clusters* was also proposed in Ref.<sup>133</sup>, aiming at developing a quantitative metric to describe diffusive heterogeneities of soft-matter media on a submicron scale.

<sup>180</sup> We mention here the recent variational Bayesian SPT-study<sup>135</sup> using the hybrid method of a gamma-mixture model and a hidden Markov model. It is aimed at recognising multiple diffusion states along particle trajectories in heterogeneous media<sup>91</sup>. Using a machine-learning approach, the time- and space-controlled regions with varying tracer diffusivities were reliably identified<sup>135</sup>.

<sup>181</sup> We note that one disadvantage of the single-trajectory-based Bayesian analysis emerges when the method is applied straightforwardly to an *ensemble* of trajectories with a *pronounced spread* of TAMSDs, as for diffusion in mucin gels at pH=2<sup>19</sup>, see Fig. 3. Here, in order to make a statement about the applicability of the FBM model for the *entire ensemble* of traces, this model must be supplemented with a set of trajectory-specific diffusivities  $p((K_\beta)_i)$  and exponents  $p(\beta_i)$ .

<sup>182</sup> Also, as quantified in Ref.<sup>49</sup>, for each diffusion model the performance and accuracy of the nested-sampling prediction of model significance are diminished for shorter trajectories. Therefore, the model-prediction results, as in Fig. 4, will change when longer traces are provided: one can expect a *stronger dominance* of one model<sup>49</sup> (results not shown). Additionally, as the level of confidence of this algorithm can vary differently for each models with trace length, the conclusions for longer tracer regarding the dominant model may also change. Moreover, for a *larger* list of possible diffusion models, relative model probabilities will likely get reduced. This is the subject of our future work.

<sup>183</sup> Clearly, fixing  $N_{\text{fit}}$  turns our results non-universal (see also Refs.<sup>107,136</sup>), inevitable in such an analysis. The initial points of  $\overline{\delta_i^2}(\Delta)$  yield the most statistically robust results for the short-time scaling behaviour<sup>66,74</sup>. Some studies reporting on optimisation of determining scaling exponents and diffusion coefficients, also in the presence of localisation errors<sup>137–139</sup>, should be mentioned here as well<sup>140–142</sup>. We note also the recent diffusivity analysis for *multistate* trajectories in heterogeneous media, i.e., when several different models of diffusion occur along a single trajectory (e.g., free and bound diffusion).<sup>143</sup>

<sup>184</sup> The distributions and correlations of scaling exponents and diffusion coefficients were uncovered for nanoparticles in mammalian cells<sup>130</sup>. We also refer to Ref.<sup>146</sup> for detection of  $p(\beta)$  and  $p(K_\beta)$  distributions for SPT data on subdiffusion of endoplasmic reticulum network. Note that pronounced  $K_\beta$ - $\beta$  *anticorrelations* were detected for active spreading of ameboid cells<sup>107</sup>.

<sup>185</sup> Additionally, the histograms for distributions of scaling exponents and diffusion coefficients are presented in Figs. A7a,b. Note that a similar splitting of particles into "ex-

ponential" and "Gaussian" subpopulations diffusing in a heterogeneous medium with space-dependent diffusivity was considered in Ref.<sup>147</sup>. We also refer to cluster-averaging and population-splitting analyses of Ref.<sup>44</sup>.

<sup>186</sup> Note that some limitations exist when evaluating EB for a *limited number* of traces. We also mention here an alternative dynamic functional-based approach to estimate non-ergodicity of a stochastic process, proposed recently in Ref.<sup>157</sup>.

<sup>187</sup> Note that the ageing properties of continuous-time random walks were examined in Refs.<sup>155,156</sup>.

<sup>188</sup> We refer to a similar TAMSD versus (PDF width) analysis performed for active diffusion of amoeboid cells in Ref.<sup>107</sup>.

<sup>189</sup> We note that *data binning* for PDFs can affect the exact values of the exponents and widths as extracted from the fit (18).

<sup>190</sup> We refer to the method study<sup>49</sup> for the detailed discussion of the criteria of model significance in the Bayesian analysis with nested sampling used here.

<sup>191</sup> Note that situations  $t < dt$  and  $t > dt$  are possible. For overdamped BM the (normalised)  $C_{dt}(t)$  function drops as a straight line from unity at  $t = 0$  to zero at  $t = dt$  and stays zero at  $t > dt$ . A similar behaviour is observed for subdiffusive continuous-time random walks<sup>74</sup>. Importantly, the fact that  $C_{dt}(t) > 0$  in the region  $0 < dt < t$  is not associated with the persistence of the process or inertia effects. As follows from Eq. (20), only at  $t > dt$  the positiveness (negativeness) of  $C_{dt}(t)$  indicates persistent motion and superdiffusion (antipersistent motion and subdiffusion).

<sup>192</sup> We mention the recent SPT analysis of diffusion of colloids in gelatin solutions<sup>159</sup> and the emergence of broader-than-Gaussian tails of the PDF of the tracers close to the critical gel point. A continuous "thickening" during the gelation transition—observed for growing *ageing times* of the samples (denoted  $t_a$ )—was shown to progressively reduce the MSD magnitude and its exponent. Note that when—following the classical studies<sup>160,161</sup>—deconvoluting the diffusivity distribution (7) conditioned with the Gaussian (5), it was shown that for longer  $t_a$  the distribution  $\pi(D)$  remains single-peaked and localised. After a critical waiting time, a "population splitting" takes place<sup>159</sup>. Namely, a second peak in  $\pi(D)$  emerges at large diffusivities and it reflects a smaller medium viscosity for this subpopulation. The conclusions of Ref.<sup>159</sup> support the findings of Ref.<sup>19</sup> regarding two separated subpopulations of tracers.

<sup>193</sup> We note that the emergence of certain "spurious" anomalous-diffusion features was discussed in Ref.<sup>110</sup> as a consequence of using conventional statistical classifiers to *strongly heterogeneous* random walks. In particular, the superstatistical approach and the autoregressive process of the first order were employed<sup>110</sup> to describe superdiffusive motion of tumour cells (breast carcinoma cells on collagen networks). A new sequential Bayesian method was proposed<sup>110</sup> to estimate the parameters of the autoregressive process (persistence and activity). The latter vary on *each* time-step along the trajectory mimicking *varying microenvironments* for cell diffusion. This renders the approach of Ref.<sup>110</sup> similar to the DD model in the current Bayesian framework.

<sup>194</sup> For instance, for financial time series longer-than-Gaussian tails in the distribution of returns occur as well. The recent Bayesian analysis with time-varying

parameters<sup>165</sup> has shown that mutual correlations of volatility and walk persistence are pronounced. Moreover, incorporating a certain *time evolution* of the model parameters can be sufficient to rationalise these tails<sup>165,166</sup>. Likewise, additional time variation  $D(t)$  can be employed for ageing diffusion in mucin gels.

<sup>195</sup> The effect of minimal trace-length  $N_p^{\min}$  varies with particle size: largest tracers are typically easier to track for longer times<sup>20</sup>. The probes of size 0.2...5  $\mu\text{m}$  were analysed in Fig. 4.3.8a,b of Ref.<sup>20</sup>. This means, however, that if long enough time series with the same  $N_p^{\min}$  are to be recorded for *different* tracer sizes, for smaller tracers this will over-represent a slower subpopulation (particles stay longer in the view-field). This might affect, e.g., the diffusivity versus particle-size relation in polymer-based solutions, often targeted in experiments<sup>27</sup>.

<sup>196</sup> Also, for tracer diffusion in mucin gels, for progressively longer trajectories of smaller tracers the respective ensemble becomes smaller than for bigger particles, for which the number of tracked particles does not drop with  $N_p^{\min}$  that rapidly. This could give rise to a paradoxical effect: in 1 wt % MUC5AC solutions at pH=2—see Fig. 4.3.8a in Ref.<sup>20</sup>—5- $\mu\text{m}$  tracers at long times show an order-of-magnitude *larger* MSD than 0.2...0.5- $\mu\text{m}$  tracers at the same conditions<sup>20</sup>. Also, as Fig. 4.3.8e of Ref.<sup>20</sup> shows, the short-time TAMSD exponent at pH=2 reveal a non-monotonic dependence with particle size. Namely, the exponent  $\langle\beta\rangle$  in (11) grows fast for small tracers and shows a weak maximum for medium-sized tracers.

### Appendix A: Bayesian model-ranking approach and parameter estimation

Below, we present some details of the Bayesian model-ranking analysis and the nested-sampling algorithm employed in the main text. We also describe some key properties of the diffusion models used in the analysis (more details are provided in the original method study<sup>49</sup>).

Using Bayes' theorem, we compute the conditional probability of a model  $M_i$  given data as<sup>50–53</sup>

$$P(M_i|\text{Data}) = P(\text{Data}|M_i)P(M_i)/P(\text{Data}). \quad (\text{A1})$$

Here,  $P(M_i|\text{Data})$  is the posterior probability,  $P(\text{Data}|M_i)$  is the marginal likelihood (or the evidence  $Z_i$ ) for  $M_i$ ,  $P(M_i)$  is the prior probability for  $M_i$ , and  $P(\text{Data})$  is the probability of the data. As all possible models ( $N_m$  in total) are initially equiprobable, they can be ranked via computing their probabilities as  $P(M_k) = Z_k / \sum_{i=1}^{N_m} Z_i$ . Each model features  $N$  parameters,  $\theta_i = \{\theta_1, \theta_2, \dots, \theta_N\}_i$ . Depending on our knowledge about their range, certain prior probability distributions are being chosen,  $\pi(\theta_i) = P(\theta_i|M_i)$ . The likelihood function of data,  $\mathcal{L}_i(\theta_i) = P(\text{Data}|\theta_i, M_i)$ , is then used to express the evidence  $Z_i$  of  $M_i$  as

$$Z_i = \int \mathcal{L}_i(\theta_i)\pi(\theta_i)d\theta_i. \quad (\text{A2})$$

To estimate the model parameters, we use the posterior probability distribution, so that from Eq. (A1) we get

$$P(\theta_i|M_i, \text{Data}) = \frac{P(\text{Data}|\theta_i, M_i)P(\theta_i|M_i)}{P(\text{Data}|M_i)} = \frac{\mathcal{L}_i(\theta_i)\pi(\theta_i)}{Z_i}, \quad (\text{A3})$$

which is used to estimate the mean and variance of each parameter of the model  $M_i$ . The evaluation of the evidence values is central for model comparison and parameter estimation results. From Eq. (A2) it follows, however, that this computation becomes—both analytically and computationally—expensive as the dimension of  $\theta_i$  increases. For this, we use the method of nested sampling<sup>52,54–56</sup> that reduces the multi-dimensional integral (A2) to a one-dimensional one<sup>49</sup>.

### Appendix B: Models of diffusion

Below, we apply the Bayesian framework to three models of diffusion used in the main text. We specify the likelihood functions, the model parameters, and their prior distributions. For parameters with large ranges, we use a prior distribution uniform on a log scale (Jeffrey's prior). In contrast, if the range of a parameter is small, a uniform prior over this range is employed. For a parameter  $\theta$  in the range  $\theta \in [\theta_{\min}, \theta_{\max}]$  the Jeffrey's prior<sup>50,57–59</sup> is

$$\pi(\theta) = \begin{cases} 1/[\theta \log(\theta_{\max}/\theta_{\min})], & \theta_{\min} < \theta < \theta_{\max} \\ 0, & \text{otherwise} \end{cases}, \quad (\text{B1})$$

while the uniform prior is given by

$$\pi(\theta) = \begin{cases} 1/[\theta_{\max} - \theta_{\min}], & \theta_{\min} < \theta < \theta_{\max} \\ 0, & \text{otherwise} \end{cases}. \quad (\text{B2})$$

(i) BM is described (in the overdamped limit) by the Langevin equation<sup>60</sup>,  $dx(t)/dt = \sqrt{2D} \times \xi(t)$ , where  $\xi(t)$  is white Gaussian noise with zero mean and auto-correlation  $\langle\xi(t_1)\xi(t_2)\rangle = \delta(t_1 - t_2)$ . As displacements  $\Delta x_j = x_j - x_{j-1}$  at the  $j$ th step are independent identically distributed random variables, we use a Gaussian likelihood function<sup>61</sup>,

$$\mathcal{L}_{\text{BM}}(\theta_{\text{BM}}) = \prod_{j=2}^{N_p} \exp\left(-\frac{(\Delta x_j)^2}{4D_j\Delta t}\right) / \sqrt{4\pi D_j\Delta t}. \quad (\text{B3})$$

Here,  $j$  is the index along the trajectory with the total number of points  $N_p$ . BM has a single parameter—the diffusion coefficient  $D_j = D$ —related to the step deviation  $\sigma$  as  $D = \sigma^2/[2(\Delta t)]$ . For the parameter  $\sigma$  we use Jeffrey's prior, Eq. (B1).

For BM with additional noise—given the actual  $x_j^{\text{act}}$  and observed particle positions  $x_j^{\text{obs}}$  at time step  $j$ —we include into  $x_j^{\text{obs}}$  a Gaussian measurement noise  $\eta_j$  (with zero mean and variance  $\langle\eta_j^2\rangle = \sigma_N^2$ ). The observed posi-

tions are then  $x_j^{\text{obs}} = x_j^{\text{act}} + \eta_j$  and the likelihood function becomes<sup>49,61,63</sup>

$$\mathcal{L}_{\text{BM+N}}(\boldsymbol{\theta}) = \prod_{j=2}^{N_p} \exp\left(-\frac{(x_j^{\text{obs}} - \tilde{x}_j)^2}{2\tilde{\sigma}_j^2}\right) / \sqrt{2\pi\tilde{\sigma}_j^2}. \quad (\text{B4})$$

Here, the sets of new variables are iteratively defined for  $2 < j \leq N_p$  as  $\tilde{x}_j = x_{j-1} - \sigma_N^2(x_{j-1} - \tilde{x}_{j-1})/\tilde{\sigma}_{j-1}^2$  and  $\tilde{\sigma}_j^2 = \sigma^2 + \sigma_N^2(2 - \sigma_N^2/\tilde{\sigma}_{j-1}^2)$ . For the initial step, at  $j = 2$ , we set  $\tilde{x}_2 = x_2$ ,  $\tilde{\sigma}_2^2 = \sigma^2 + 2\sigma_N^2$ . In addition to  $D$ , for noisy BM we use a uniform prior (B2) for  $\sigma_N$ .

(ii) FBM obeys the equation  $dx(t)/dt = \xi_{\text{fGn}}(t)$ , where  $\xi_{\text{fGn}}(t)$  is the fractional Gaussian noise with zero mean and long-ranged correlations<sup>64,65</sup>,

$$\langle \xi_{\text{fGn}}(t_1)\xi_{\text{fGn}}(t_2) \rangle = 2H(2H-1)D_H \times |t_1 - t_2|^{2(H-1)}. \quad (\text{B5})$$

Here  $t_1 \neq t_2$ , the angular brackets denote averaging over the noise,  $D_H$  is the generalised diffusion coefficient, and  $H$  is the Hurst exponent. Two parameters of FBM— $D_H$  and  $H$ —are to be determined. The step deviation  $\sigma_H$  obeys the relation  $D_H = \sigma_H^2/[2(\Delta t)^{2H}]$ . As possible  $\sigma_H$  values vary in a wide range, Jeffrey's prior (B1) is used for  $\sigma_H$ . For a limited range of Hurst exponents,  $H \in [0, 1]$ , a uniform prior (B2) is used.

We derive for the FBM model a quadratic form similar to (B4). For this, for  $N_p$  positions at evenly spaced time intervals (the time-step is  $\Delta t$ ), the displacements after  $n$  diffusion steps  $\Delta x_n = x_n - x_{n-1}$  have the autocovariance function<sup>61,63</sup>  $\gamma(k) = \langle \Delta x_n \times \Delta x_{n+k} \rangle = D_H(\Delta t)^{2H} [|k+1|^{2H} + |k-1|^{2H} - 2|k|^{2H}]$ . Here, the index  $k$  denotes the step number. This function only depends on the time-step difference,  $k$ , see Ref.<sup>66</sup>. From displacements along the trajectory, the column-vector  $\Delta \mathbf{x}_{(N_p-1)}$  and its transpose  $\Delta \mathbf{x}_{(N_p-1)}^T$  are created. The likelihood function is constructed as<sup>49,63</sup>

$$\mathcal{L}_{\text{FBM}}(\boldsymbol{\theta}) = \frac{\exp\left(-\frac{1}{2}\Delta \mathbf{x}_{(N_p-1)}^T \boldsymbol{\Gamma}_{(N_p-1)}^{-1} \Delta \mathbf{x}_{(N_p-1)}\right)}{(2\pi)^{N/2} |\boldsymbol{\Gamma}_{(N_p-1)}|^{1/2}} \quad (\text{B6})$$

where  $\boldsymbol{\Gamma}_{(N_p-1)}^{-1}$  is the inverse of the  $(N_p - 1) \times (N_p - 1)$  covariance matrix with the elements  $\gamma(m - n)$  and determinant  $|\boldsymbol{\Gamma}_{(N_p-1)}|$ .

We also consider the model of noisy FBM for which the displacements have the autocovariance function<sup>63</sup>

$$\gamma^{\text{obs}}(k) = \begin{cases} \gamma^{\text{act}}(0) + 2\sigma_N^2, & \text{for } k = 0 \\ \gamma^{\text{act}}(1) - \sigma_N^2, & \text{for } k = 1 \\ \gamma^{\text{act}}(0), & \text{for } 1 < k < (N_p - n - 1) \end{cases} \quad (\text{B7})$$

The likelihood function for the noisy FBM model is<sup>49,63</sup>

$$\begin{aligned} \mathcal{L}_{\text{FBM+N}}(\boldsymbol{\theta}) &= \frac{\exp\left(-\frac{1}{2}\left(\Delta \mathbf{x}_{(N_p-1)}^{\text{obs}}\right)^T \left(\boldsymbol{\Gamma}_{(N_p-1)}^{\text{obs}}\right)^{-1} \left(\Delta \mathbf{x}_{(N_p-1)}^{\text{obs}}\right)\right)}{(2\pi)^{N/2} \left|\boldsymbol{\Gamma}_{(N_p-1)}^{\text{obs}}\right|^{1/2}}, \end{aligned} \quad (\text{B8})$$

where  $\left(\boldsymbol{\Gamma}_{(N_p-1)}^{\text{obs}}\right)_{m,n} = \gamma^{\text{obs}}(m - n)$ . The model of FBM with additional noise has three parameters: the step deviation  $\sigma_H$ , the Hurst index  $H$ , and the strength  $\sigma_N$  of the measurement noise. For  $\sigma_H$  we use (B1), while for  $H$  and  $\sigma_N$  (B2) is used as a prior.

(iii) The minimal model of DD obeys the system of stochastic differential equations<sup>49,67</sup>

$$dx(t)/dt = \sqrt{2D(t)} \times \xi(t) \quad (\text{B9a})$$

$$D(t) = Y^2(t) \quad (\text{B9b})$$

$$dY(t)/dt = -Y(t)/\tau + \varepsilon \times \bar{\eta}(t). \quad (\text{B9c})$$

Here,  $x(t)$  is the position,  $D(t)$  is the time-dependent diffusivity (in terms of auxiliary variable  $Y(t)$  given by the OU process<sup>68,69</sup>),  $\varepsilon$  is the amplitude of white Gaussian noise, and  $\tau$  is the relaxation time. The parameters of the DD model ( $(N_p + 1)$  in total) are  $\boldsymbol{\theta}_{\text{DD}} = [\tau, D_*, D_1, D_2, \dots, D_{(N_p-1)}]$ . Here,  $D_*$  is the characteristic diffusivity and  $\{D_1, D_2, \dots, D_{N_p-1}\}$  are the instantaneous diffusion coefficients at times  $\left\{\frac{t_1+t_2}{2}, \frac{t_2+t_3}{2}, \dots, \frac{t_{(N_p-1)}+t_{N_p}}{2}\right\}$  (computed for each particle trajectory). The diffusivities at these times are  $\{Y_1^2, Y_2^2, \dots, Y_{(N_p-1)}^2\}$ .

For the parameters  $\tau$  and  $D_*$  we use Jeffrey's prior (B1). For  $Y_1$  we choose the prior from the equilibrium distribution of the OU process<sup>49,67</sup> as  $\pi(Y_1|D_*) = (\pi D_*)^{-1/2} \exp(-Y_1^2/D_*)$ . For all the other  $Y_j$  we use the OU Gaussian displacement distribution<sup>49,67</sup> and a Gaussian prior. Thus, for an arbitrary  $k$  we define the set of  $\{Y_{|k|}\} \equiv \{Y_1, Y_2, \dots, Y_{k-1}, Y_{k+1}, \dots, Y_{(N_p-1)}\}$  (not containing the value  $Y_k$ ). For  $\{Y_{|1|}\}$  the prior is<sup>49</sup>

$$\pi(\{Y_{|1|}\}|\{\tau, D_*, Y_1\}) = \frac{\exp\left(-\frac{\sum_{l=2}^{N_p-1} (Y_l - Y_{l-1} e^{-\Delta t/\tau})^2}{D_*(1 - e^{-2\Delta t/\tau})}\right)}{[\pi D_* \{1 - e^{-2\Delta t/\tau}\}]^{\frac{N_p-2}{2}}}. \quad (\text{B10})$$

The likelihood function for the DD model can be written similarly to that of BM, Eq. (B3). As the position increments  $\Delta x_j$  are independent random variables, the likelihood is given by the product of Gaussian likelihoods for each increment<sup>49</sup>, namely

$$\mathcal{L}_{\text{DD}}(\boldsymbol{\theta}) = \prod_{j=1}^{N_p-1} \exp\left(-\frac{(\Delta x_j)^2}{4D_j\Delta t}\right) / \sqrt{4\pi D_j\Delta t}.$$

### Appendix C: Supplementary figures

Below we present additional figures supporting the claims in the main text of the paper.

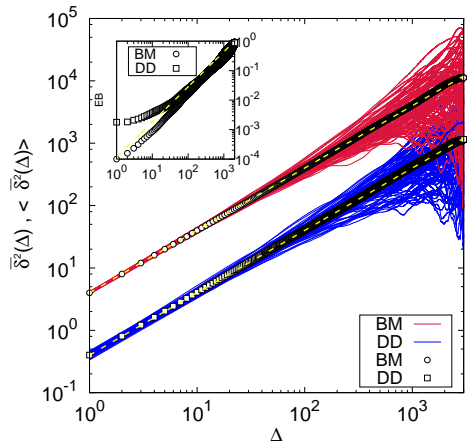


FIG. A1: Distribution of  $N = 10^2$  TAMSD trajectories of  $T = 3000$  points long for the models of BM (red curves) and DD (blue curves). The ensemble-averaged quantities are shown by the symbols. The inset shows the evolution of ergodicity breaking parameters for these two models versus lag time  $\Delta$ . Parameters:  $D = 1$ ,  $\Delta t = 1$  (for the BM model) and  $\tau = 5$ ,  $D_* = 0.2$ ,  $\Delta t = 1$  (for the DD model), see also Ref.<sup>49</sup> for the details of the Bayesian analysis. The image is reproduced from Ref.<sup>49</sup> with permission from the Royal Society of Chemistry.

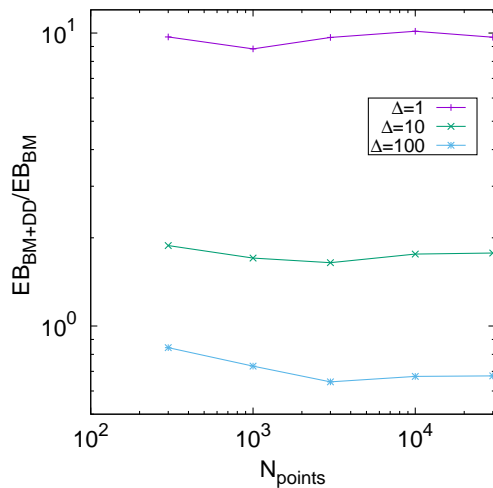


FIG. A2: Ergodicity breaking parameter for the DD model, normalised to the BM values and plotted versus lag time  $\Delta$ , as obtained from computer simulations, see Ref.<sup>49</sup>. The trace length is  $T = 3 \times 10^4$  and lag time varies. Other parameters are the same as in Fig. A1.

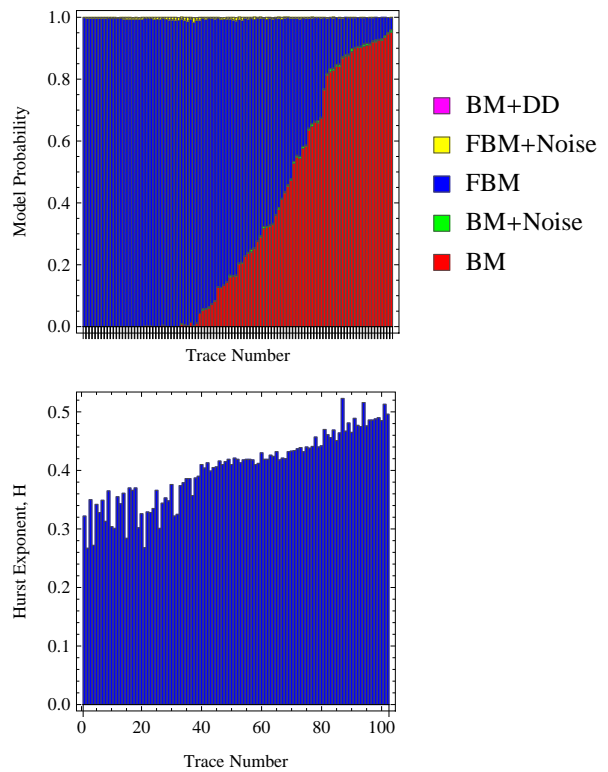


FIG. A3: The same as in Fig. 4 but at pH=4, with  $N = 102$  trajectories<sup>19</sup>.

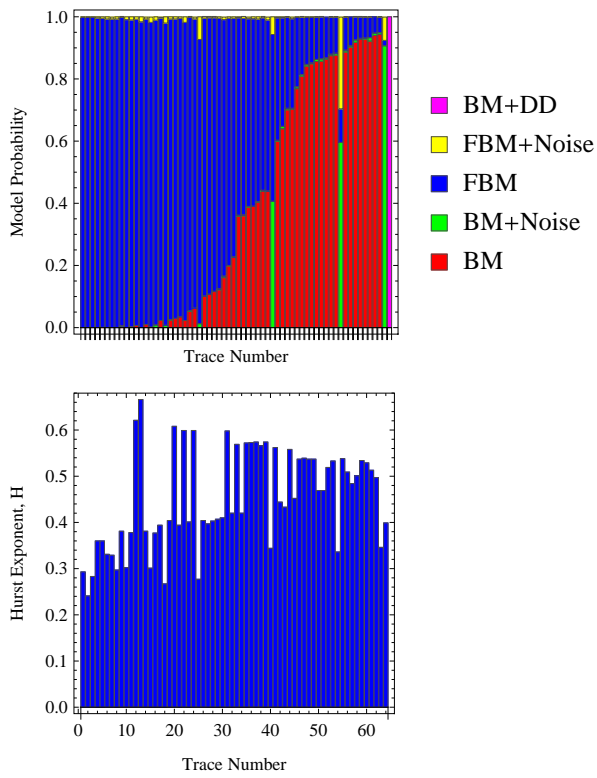


FIG. A4: The same as in Fig. 4 but at pH=2 (experiment #1 of Ref.<sup>19</sup> with  $N = 64$  traces).

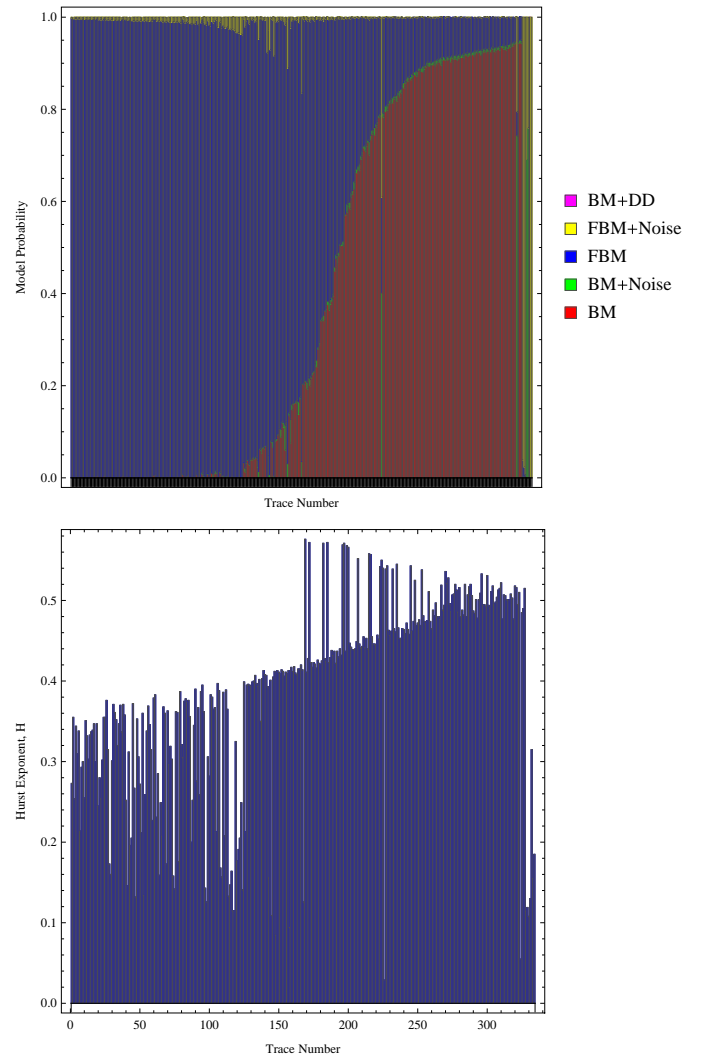


FIG. A5: The same as in Fig. 4 but at pH=2 (experiment #3 of Ref.<sup>19</sup> containing  $N = 334$  traces).

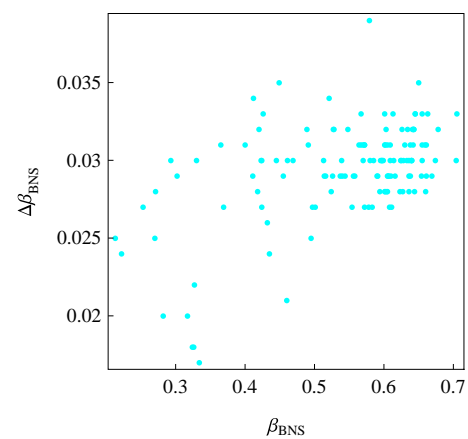


FIG. A6: Correlations of Bayesian scaling exponents and errors in their determination. The data of tracer diffusion in gels at pH=2 from the experiment #2 of Ref.<sup>19</sup> were used.

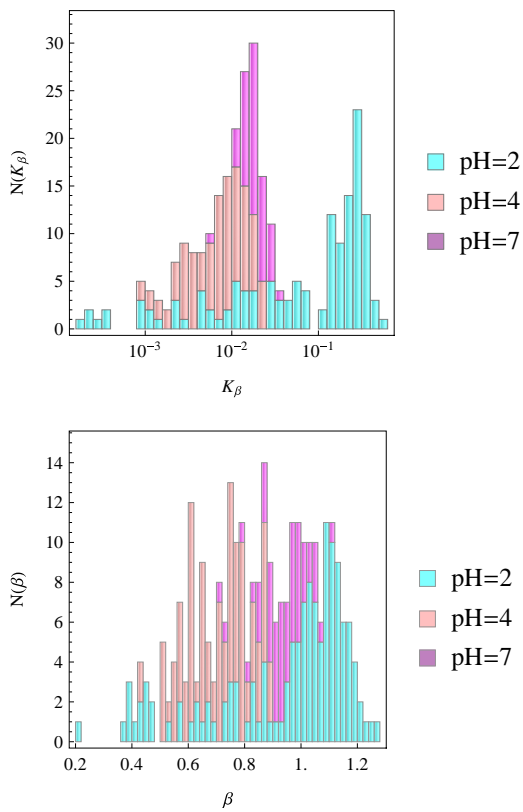


FIG. A7: *Stacked* histograms of distributions of initial scaling exponents of TAMSDs and respective diffusion coefficients (see Eq. (11)), computed for the data sets of Fig. 7. Data bars at different pH values do not overlap in these histograms.

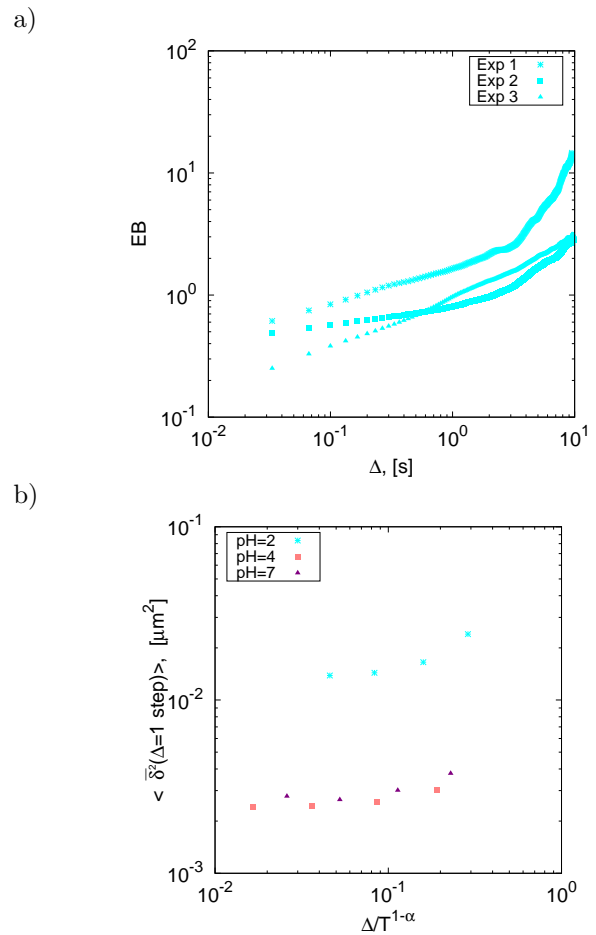


FIG. A8: Panel (a): Comparison of the ergodicity breaking parameters for the data sets of Ref.<sup>19</sup> at pH=2 with different number of trajectories ( $N = 64, 134, \text{ and } 334$ ). Panel (b): the magnitude of the mean TAMSD at  $\Delta = 1$  step for the data sets of Fig. 3, plotted for varying trajectory length ( $T = 10, 30, 100, 300$  points) for pH=2, 4, and 7. At longer  $T$  no significant ageing dependence is observed. Coding for colours is the same as in Fig. 3.

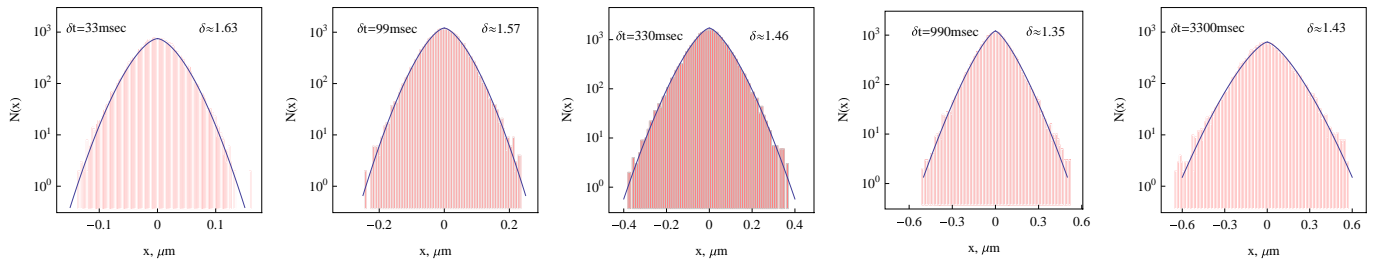


FIG. A9: The same as in Fig. 9 but for pH=4 data set of Ref.<sup>19</sup>.

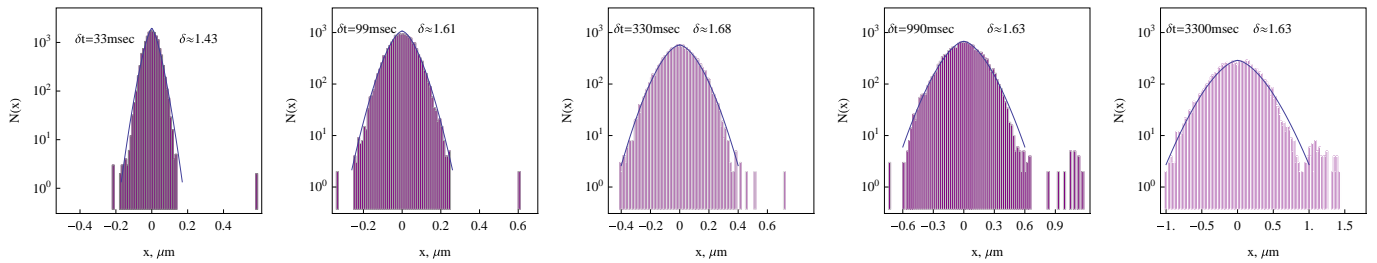


FIG. A10: The same as in Fig. 9 but for pH=7. Note that the entire data sets of displacements are presented here, including some statistically insignificant rare outliers at relatively large tracer displacements.

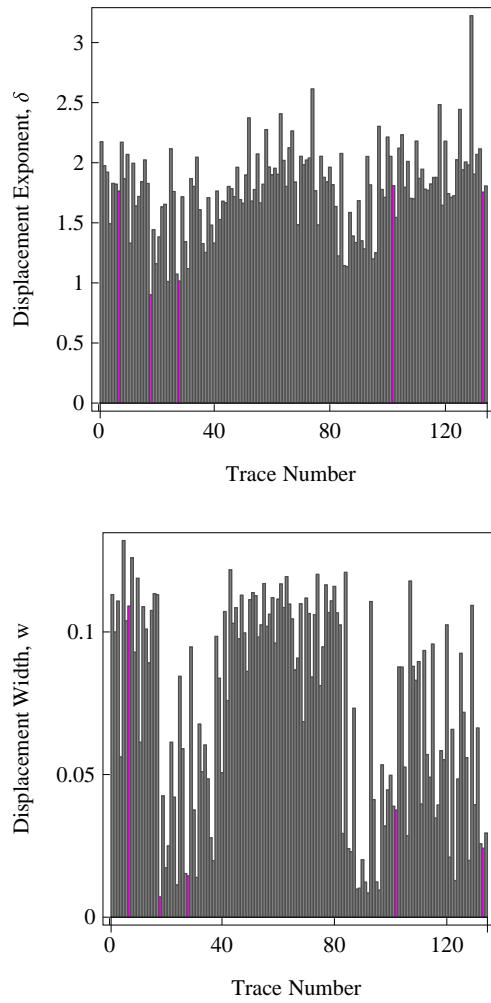


FIG. A11: Distribution of scaling exponents  $\delta$  and widths  $w$  of tracer displacement distributions, see the fit of Eq. (18), for individual tracers as measured at pH=2 in experiment #2 of Ref.<sup>19</sup>. The traces have the same (original) order in both panels. The trajectories dominated by the DD model are in magenta (the same colour coding as in Fig. 5).

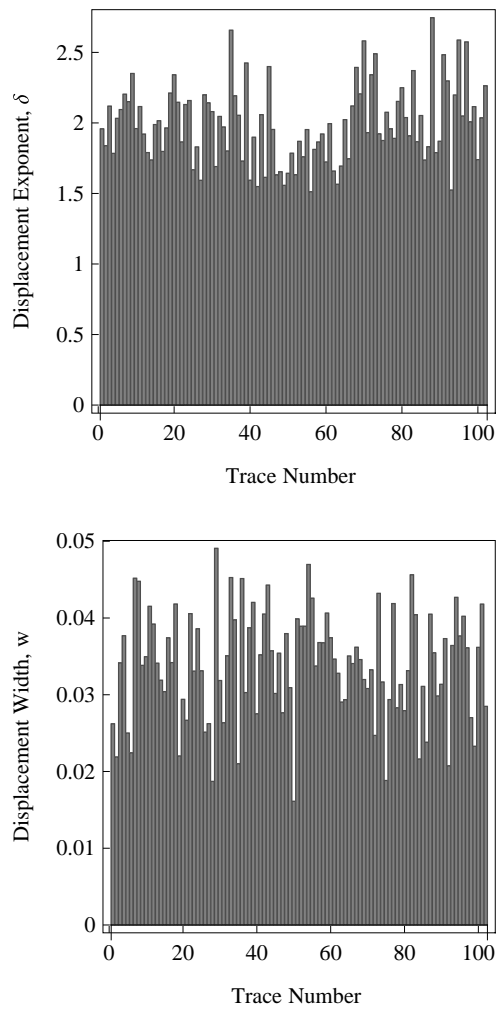


FIG. A12: The same as in Fig. A11 but for  $N = 102$  tracer trajectories at pH=4 in Ref.<sup>19</sup>.

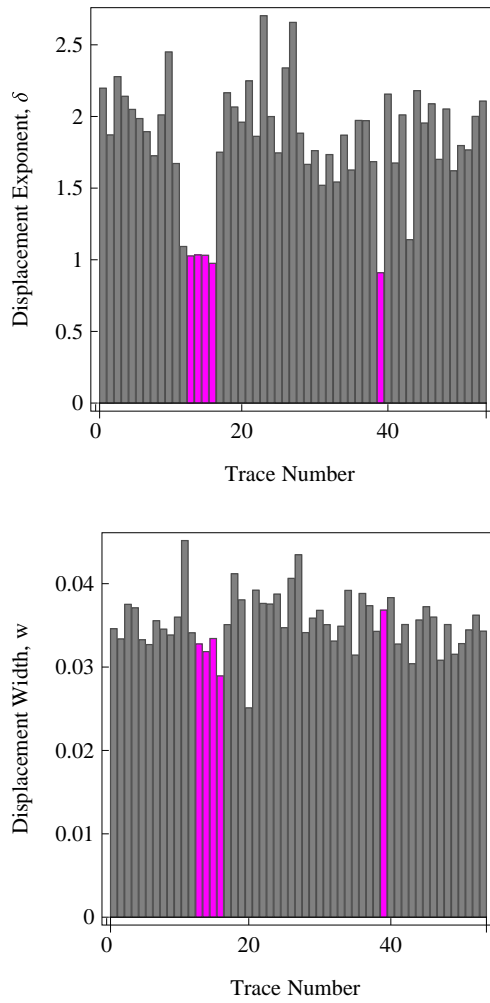


FIG. A13: The same as in Fig. A11 but computed for tracer trajectories in mucin gels at pH=7, as measured in Ref.<sup>19</sup>.

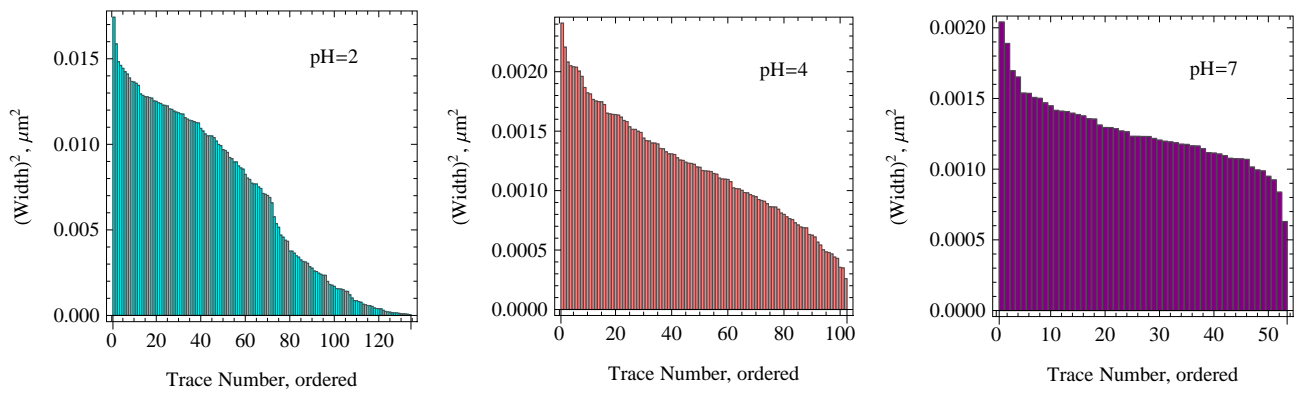


FIG. A14: Histograms of the width of tracer displacement distributions for single trajectories, see Eq. (18), as obtained by fitting  $\delta t = 33$  msec data of Ref.<sup>19</sup> for different pH values (as indicated in the panels). The colours are the same as in Fig. 3.

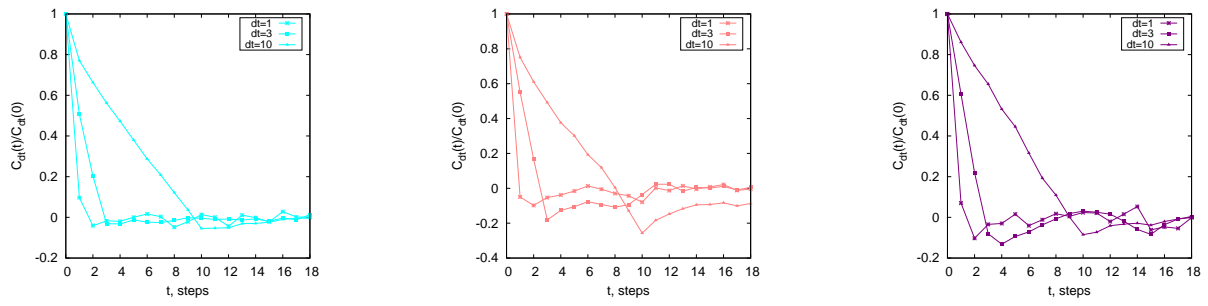


FIG. A15: Displacement autocorrelation functions (20) computed for varying time shifts (the values are given in the legends). The colour-coding scheme for pH=2, 4, and 7 (for the panels from left to right, respectively) is the same as in Fig. 3.

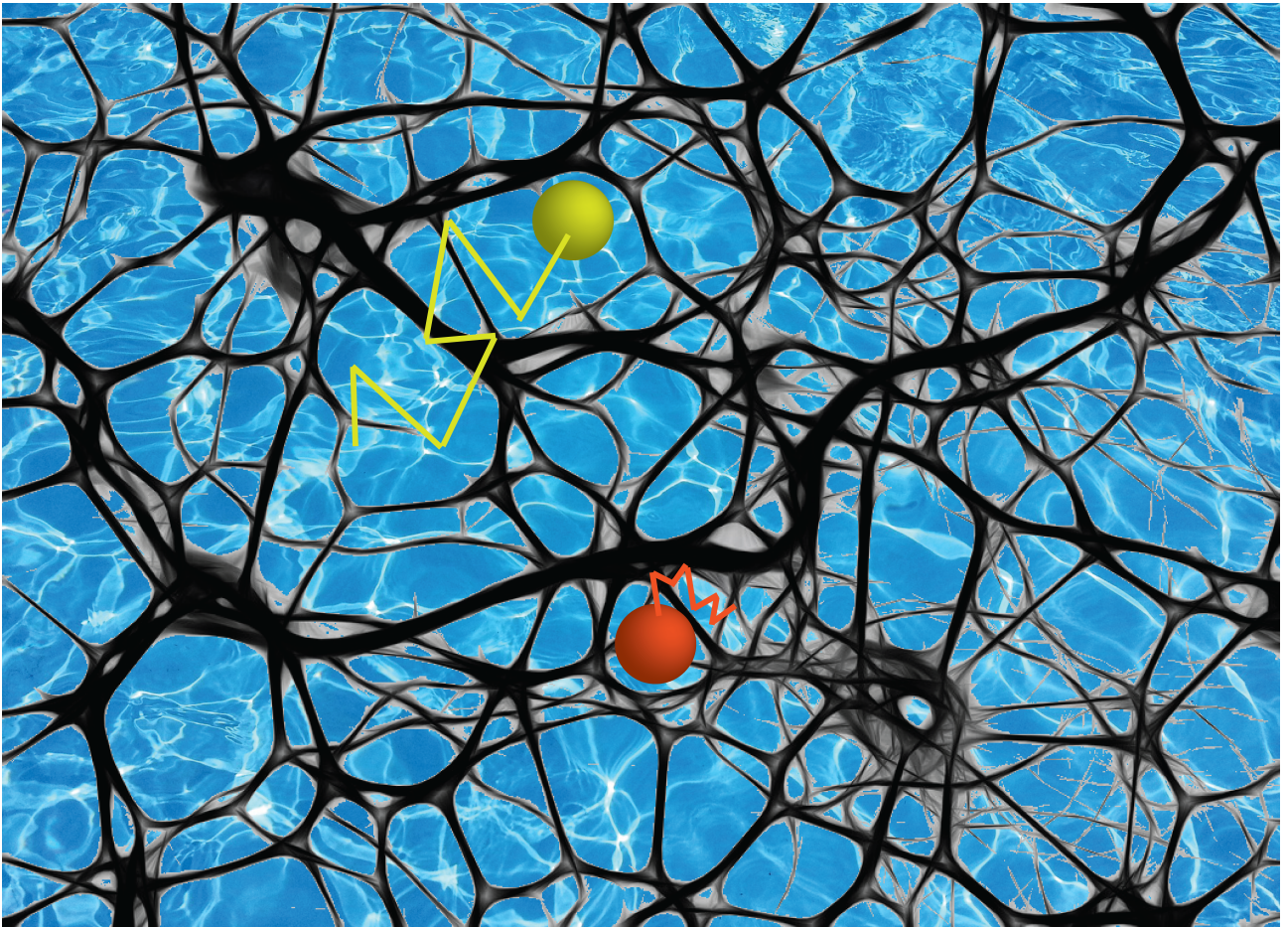


FIG. TOC1: TOC image (source images courtesy pixabay.com)